Light nuclei and hypernuclei from quantum chromodynamics in the limit of SU(3) flavor symmetry

S. R. Beane,[1] E. Chang,[2] S. D. Cohen,[3] W. Detmold,[4,5] H. W. Lin,[3] T. C. Luu,[6] K. Orginos,[4,5]
A. Parreño,[2] M. J. Savage,[3] and A. Walker-Loud[7,8]

(NPLQCD Collaboration)

[1]*Department of Physics, University of New Hampshire, Durham, New Hampshire 03824-3568, USA*
[2]*Departament d'Estructura i Constituents de la Matèria, Institut de Ciències del Cosmos (ICC),
Universitat de Barcelona, Martí i Franquès 1, E08028 Spain*
[3]*Department of Physics, University of Washington, Box 351560, Seattle, Washington 98195, USA*
[4]*Department of Physics, College of William and Mary, Williamsburg, Virginia 23187-8795, USA*
[5]*Jefferson Laboratory, 12000 Jefferson Avenue, Newport News, Virginia 23606, USA*
[6]*N Section, Lawrence Livermore National Laboratory, Livermore, California 94551, USA*
[7]*Lawrence Berkeley National Laboratory, Berkeley, California 94720, USA*
[8]*Department of Physics, University of California, Berkeley, California 94720, USA*

The binding energies of a range of nuclei and hypernuclei with atomic number $A \leq 4$ and strangeness $|s| \leq 2$, including the deuteron, dineutron, H-dibaryon, ^{3}He, $^{3}_{\Lambda}$He, ^{4}He, $^{4}_{\Lambda}$He, and $^{4}_{\Lambda\Lambda}$He, are calculated in the limit of flavor-SU(3) symmetry at the physical strange-quark mass with quantum chromodynamics (without electromagnetic interactions). The nuclear states are extracted from lattice QCD calculations performed with $n_f = 3$ dynamical light quarks using an isotropic clover discretization of the quark action in three lattice volumes of spatial extent $L \sim 3.4$ fm, 4.5 fm, and 6.7 fm, and with a single lattice spacing $b \sim 0.145$ fm.

I. INTRODUCTION

The structure and interactions of the light nuclei have been the focus of experimental and theoretical explorations since the infancy of nuclear physics. Yet more than 100 years later, and despite having made remarkable progress in describing these systems in terms of nuclear forces that are well-constrained by experiment, we remain unable to predict the binding and interactions of any given nucleus with reliable estimates of the associated uncertainties. It has long been accepted that quantum chromodynamics (QCD) and the electroweak interactions produce the nuclear forces, and consequently are responsible for the structure and interactions of all nuclei. Unfortunately, the complexity of the QCD vacuum has so far prevented the calculation of low-energy and medium-energy nuclear systems directly from QCD. Beyond recovering the results of decades of experimental investigation, it is crucial to establish and verify tools with which to perform such calculations, with quantifiable uncertainties, in order to determine the properties and structure of exotic nuclei and of matter in extreme environments or in kinematic regimes where experiments are not possible or practical.

The only known way to calculate the low-energy properties of hadronic and nuclear systems rigorously is lattice QCD (LQCD). In LQCD calculations, the quark and gluon fields are defined on a discretized space-time of finite volume, and the path integral over the fields is evaluated numerically. While LQCD calculations deviate from those of QCD because of the finite distance between points of the grid (lattice spacing) and the finite volume of the grid (lattice volume), such deviations can be systematically removed by reducing the lattice spacing, increasing the lattice volume, and extrapolating to the continuum and infinite-volume limits using the known dependences determined with effective field theory (EFT). Calculation of important quantities in nuclear physics using LQCD is only now becoming practical, with first calculations of simple multibaryon interactions being recently performed, although not at the physical values of the light-quark masses. Early exploratory quenched calculations of the nucleon-nucleon (NN) scattering lengths [1,2] performed more than a decade ago have been superseded by $n_f = 2 + 1$ calculations within the past few years [3,4] (and added to by further quenched calculations [5–7]). Further, the first quenched calculations of the deuteron [8], ^{3}He, and ^{4}He [9] have been performed, along with $n_f = 2$ and $n_f = 2 + 1$ calculations of ^{3}He [10,11] and $n_f = 2 + 1$ multibaryon systems containing strange quarks [11]. In addition, efforts to explore nuclei and nuclear matter using the strong coupling limit of QCD have led to some interesting observations [12]. Recently, $n_f = 2 + 1$ calculations [13,14] and $n_f = 3$ calculations [15–17] have provided evidence that the H-dibaryon (with the quantum numbers of $\Lambda\Lambda$) is bound at a pion mass of

$m_\pi \sim 390$ MeV with the physical value of the strange-quark mass [13,14], and over a range of SU(3)-degenerate light-quark masses with $m_\pi \sim 469$–1171 MeV [15,16]. Extrapolations to the physical light-quark masses suggest that a weakly bound H-dibaryon, or a near-threshold resonance, exists in this channel [14,18–20]. We have searched for bound states in other channels at $m_\pi \sim 390$ MeV [13,14], and evidence has been found for a bound state in the strangeness-4 $\Xi^0\Xi^0$ system. This is consistent with model-dependent and EFT predictions of a bound state in this channel at the physical pion mass [21–23]. In addition to the identification of bound states, calculations of hyperon-nucleon scattering extrapolated to the physical pion mass (using leading-order EFT) have been performed and directly compared with the results of phase-shift analyses of experimental data [24].

In this work we focus on the lightest nuclei and hyper-nuclei and present results of the first LQCD calculations of a number of *s*-shell nuclei and hypernuclei with $A \leq 5$, including ^{3}He, $^3_\Lambda$He, $^4_\Lambda$He, $^4_{\Lambda\Lambda}$He, and a five-body state $\Lambda\Xi^0 pnn$ in the limit of exact SU(3)-flavor symmetry (and consequently, exact isospin symmetry). Hypernuclear spectroscopy is enjoying an experimental renaissance with ongoing and planned programs at DAΦNE, FAIR, Jefferson Lab, J-PARC, and Mainz, providing motivation for enhanced theoretical efforts (for a recent review, see Ref. [25]). Our LQCD calculations are performed using an isotropic clover quark action at the SU(3)-flavor symmetric point corresponding to the physical strange-quark mass, with $m_\pi = m_K = m_\eta \sim 800$ MeV. Three lattice volumes have been employed with a spatial extent of $L \sim 3.4$ fm, 4.5 fm, and 6.7 fm, and calculations of systems with nonzero total momentum (boosted systems) have been performed to investigate the volume dependence of binding energies [26,27]. As this is the first calculation of hypernuclei with baryon number $A > 2$, it is prudent to establish benchmarks for future works. The spectra of nuclei will have the simplest structure at the SU(3) symmetry point, where the up, down, and strange quarks have the same mass, allowing for a relatively uncomplicated analysis. While any common light-quark mass could have been used, the physical value of the strange-quark mass was chosen so that only the (common) up and down quark masses deviated from their physical values, and also so that the four- and five-baryon

systems would be well contained within the three selected lattice volumes. Further, such a large value of the pion mass, combined with the temporal extent of the gauge-field configurations, strongly suppresses thermal effects that are present in all calculations and can provide a systematic uncertainty in extracting the small energy differences present in nuclei. Only one relatively coarse lattice spacing, $b \sim 0.145$ fm, has been used in the calculations, dictated by the available computational resources, and therefore, an extrapolation to the continuum has not been performed. Further, extrapolations to the physical light-quark masses have not been attempted because the quark-mass dependences of the energy levels in the light nuclei are not known. Future calculations at smaller lattice spacings and at lighter quark masses will facilitate such extrapolations and lead to first predictions for the spectrum of light nuclei with completely quantified uncertainties that can be compared with experiment.

II. LATTICE QCD CALCULATIONS

A. Computational overview

Three ensembles of isotropic gauge-field configurations, generated with a tadpole-improved Lüscher-Weisz gauge action and a clover fermion action [28], are used in this work. This particular lattice-action setup follows closely the anisotropic clover action of the ensembles generated by the JLab group that we have used in our previous calculations [4,11,13,14,18,24]. The parameter tuning and scaling properties of this action will be discussed elsewhere [29]. One level of stout smearing [30] with $\rho = 0.125$ and tadpole-improved tree-level clover coefficient $c_{\text{SW}} = 1.2493$ are used in the gauge-field generation. Studies [29,31,32] of the partially conserved axial-current relation in the Schrödinger functional indicate that this choice is consistent with vanishing $\mathcal{O}(b)$ violations, leading to discretization effects that are essentially $\mathcal{O}(b^2)$. The parameters of the ensembles are listed in Table I, and further details will be presented elsewhere [29]. As multibaryon systems are the focus of this work, relatively large lattice volumes are employed for the calculations, with correspondingly large values of $m_\pi L$ and $m_\pi T$. To convert the calculated (binding) energies from lattice units (l.u.) into physical units (MeV), a lattice spacing of

TABLE I. Parameters of the ensembles of gauge-field configurations and of the measurements used in this work. The lattices have dimension $L^3 \times T$, a lattice spacing b, and a bare quark mass bm_q (in lattice units) generating a pion of mass m_π. N_{src} light-quark sources are used (as described in the text) to perform measurements on N_{cfg} configurations in each ensemble. The three uncertainties associated with the pion mass are statistical, fitting systematic, and that associated with the lattice spacing, respectively.

Label	L/b	T/b	β	bm_q	b [fm]	L [fm]	T [fm]	m_π [MeV]	$m_\pi L$	$m_\pi T$	N_{cfg}	N_{src}
A	24	48	6.1	-0.2450	0.145	3.4	6.7	806.5(0.3)(0)(8.9)	14.3	28.5	3822	72
B	32	48	6.1	-0.2450	0.145	4.5	6.7	806.9(0.3)(0.5)(8.9)	19.0	28.5	3050	48
C	48	64	6.1	-0.2450	0.145	6.7	9.0	806.7(0.3)(0)(8.9)	28.5	38.0	1905	54

$b = 0.1453(16)$ fm has been determined for these ensembles of gauge-field configurations from the Υ spectrum [33].

The N_{cfg} gauge configurations in each of the ensembles are separated by at least 10 hybrid Monte Carlo evolution trajectories to reduce autocorrelations, and an average of N_{src} measurements are performed on each configuration. The quark propagators were constructed with gauge-invariant Gaussian-smeared sources with stout-smeared gauge links. These sources are distributed over a grid, the center of which is randomly distributed within the lattice volume on each configuration, and the quark propagators are computed using the BiCGstab algorithm with a tolerance of 10^{-12} in double precision. The quark propagators, either unsmeared or smeared at the sink using the same parameters as used at the source, give rise to two sets of correlation functions for each combination of source and sink interpolating fields, labeled as SP and SS, respectively. The propagators are contracted to form baryon blocks projected to fixed momentum at the sink for use in the calculation of the correlation functions to be described below. The blocks are defined as

$$\mathcal{B}_H^{ijk}(\mathbf{p}, t; x_0) = \sum_{\mathbf{x}} e^{i\mathbf{p}\cdot\mathbf{x}} S_i^{(f_1), i'}(\mathbf{x}, t; x_0) S_j^{(f_2), j'}$$
$$\times (\mathbf{x}, t; x_0) S_k^{(f_3), k'}(\mathbf{x}, t; x_0) b_{i'j'k'}^{(H)}, \quad (1)$$

where $S^{(f)}$ is a quark propagator of flavor f, and the indices are combined spin-color indices running over $i = 1, \ldots, N_c N_s$.[1] The choice of the f_i and the tensor $b^{(H)}$ depend on the spin and flavor of the baryon, H, under consideration. For our calculations we used the local interpolating fields constructed in Ref. [34], restricted to those that contain only upper spin components (in the Dirac spinor basis). This choice results in the simplest interpolating fields that also have the best overlap with the octet-baryon ground states. Blocks are constructed for all lattice momenta $|\mathbf{p}|^2 < 4$, allowing for the study of multibaryon systems with zero or nonzero total momentum and with nontrivial spatial wave functions.

B. Multibaryon interpolating operators and contractions

To define correlation functions for the multihadron systems, interpolating operators with well defined quantum numbers at the source and sink are constructed. As we intend to perform calculations away from the SU(3)-flavor symmetry limit at lighter quark masses, the quantum numbers of parity π, angular momentum $\mathbf{J}^2$ and J_z, strangeness s, baryon number (atomic number) A, and isospin $\mathbf{I}^2$ and I_z

TABLE II. The baryon number A, strangeness s, total isospin I, total spin and parity J^π quantum numbers of the states, and interpolating operators studied in the current work. For each set of quantum numbers, the SU(3) irreps that are possible to construct with local interpolating operators are listed. The last column lists the SU(3) irrep(s) of the interpolating operators used in this work, and the dashes indicate that the state is inferred from other states using SU(3) symmetry.

Label	A	s	I	J^π	Local SU(3) irreps	This work
N	1	0	1/2	$1/2^+$	**8**	**8**
Λ	1	-1	0	$1/2^+$	**8**	**8**
Σ	1	-1	1	$1/2^+$	**8**	**8**
Ξ	1	-2	1/2	$1/2^+$	**8**	**8**
d	2	0	0	1^+	$\overline{\mathbf{10}}$	$\overline{\mathbf{10}}$
nn	2	0	1	0^+	**27**	**27**
$n\Lambda$	2	-1	1/2	0^+	**27**	**27**
$n\Lambda$	2	-1	1/2	1^+	$\mathbf{8}_A, \overline{\mathbf{10}}$	-
$n\Sigma$	2	-1	3/2	0^+	**27**	**27**
$n\Sigma$	2	-1	3/2	1^+	**10**	**10**
$n\Xi$	2	-2	0	1^+	$\mathbf{8}_A$	$\mathbf{8}_A$
$n\Xi$	2	-2	1	1^+	$\mathbf{8}_A, \mathbf{10}, \overline{\mathbf{10}}$	-
H	2	-2	0	0^+	**1, 27**	**1, 27**
^{3}H, ^{3}H	3	0	1/2	$1/2^+$	$\overline{\mathbf{35}}$	$\overline{\mathbf{35}}$
$_\Lambda^3$H$(1/2^+)$	3	-1	0	$1/2^+$	$\overline{\mathbf{35}}$	-
$_\Lambda^3$H$(3/2^+)$	3	-1	0	$3/2^+$	**10**	**10**
$_\Lambda^3$He,$_\Lambda^3\tilde{\text{H}}$, $nn\Lambda$	3	-1	1	$1/2^+$	$\mathbf{27}, \overline{\mathbf{35}}$	$\mathbf{27}, \overline{\mathbf{35}}$
$_\Sigma^3$He	3	-1	1	$3/2^+$	**27**	**27**
^{4}He	4	0	0	0^+	$\overline{\mathbf{28}}$	$\overline{\mathbf{28}}$
$_\Lambda^4$He, $_\Lambda^4$H	4	-1	1/2	0^+	$\overline{\mathbf{28}}$	-
$_{\Lambda\Lambda}^4$He	4	-2	1	0^+	$\mathbf{27}, \overline{\mathbf{28}}$	$\mathbf{27}, \overline{\mathbf{28}}$
$\Lambda\Xi^0 pnn$	5	-3	0	$3/2^+$	$\overline{\mathbf{10}} + \cdots$	$\overline{\mathbf{10}}$

are used to define the interpolating operators.[2] These interpolating operators are first constructed recursively at the hadronic level from the octet-baryon field operators using the appropriate group products (Clebsch-Gordan coefficients for isospin and angular momentum) to build an outer product wave function |space⟩ ⊗ |ang.mom.⟩ ⊗ |isospin⟩ ⊗ |parity⟩ of given strangeness and baryon number. This approach is similar to that used in Ref. [34] in the context of excited baryons. The baryons within this wave function are then replaced by appropriate quark-level wave functions, of which there are, in principle, multiple choices, and then a quark-level antisymmetrization is performed (as color is included in the quark level wave functions). A similar approach has been used to investigate the $\Omega^- \Omega^-$ system [35].

The quantum numbers defining the systems that we discuss in this paper are shown in Table II. States are given a

---

[1]To be specific, for a quark spin component $i_s = 1, \ldots, N_s$ and color component $i_c = 1, \ldots, N_c$, the combined index $i = N_c(i_s - 1) + i_c$.

[2]For calculations restricted to the SU(3)-flavor symmetric limit, it would also be advantageous to work directly with SU(3) irreducible representations.

TABLE III.   The pion energy (l.u.) as a function of momentum (l.u.), $|\mathbf{P}| = (\frac{2\pi}{L})|\mathbf{n}|$, calculated on each ensemble of gauge-field configurations. The infinite-volume pion mass, determined by fitting the expression in Eq. (2), is provided in the last row. The first uncertainty is statistical, and the second is the fitting systematic.

Ensemble	$|\mathbf{n}| = 0$	$|\mathbf{n}|^2 = 1$	$|\mathbf{n}|^2 = 2$	$|\mathbf{n}|^2 = 3$	$|\mathbf{n}|^2 = 4$	$|\mathbf{n}|^2 = 5$
$24^3 \times 48$	0.59389(18)(18)	0.64652(16)(19)	0.69482(17)(29)	0.73971(20)(36)	0.77800(30)(72)	0.81946(36)(78)
$32^3 \times 48$	0.59445(15)(17)	0.62474(15)(18)	0.65326(16)(20)	0.68099(18)(25)	0.70672(19)(28)	0.73194(22)(31)
$48^3 \times 64$	0.59403(16)(14)	0.60768(16)(15)	0.62101(18)(17)	0.63403(19)(20)	0.64667(21)(24)	0.65915(24)(28)
$L = \infty$	0.59426(12)(11)					

TABLE IV.   The ground-state octet-baryon energy (l.u.) as a function of momentum (l.u.), $|\mathbf{P}| = (\frac{2\pi}{L})|\mathbf{n}|$, calculated on each ensemble of gauge-field configurations. The infinite-volume baryon mass, determined by fitting the expression in Eq. (2), is provided in the last row. The first uncertainty is statistical, and the second is the fitting systematic.

Ensemble	$|\mathbf{n}| = 0$	$|\mathbf{n}|^2 = 1$	$|\mathbf{n}|^2 = 2$	$|\mathbf{n}|^2 = 3$	$|\mathbf{n}|^2 = 4$	$|\mathbf{n}|^2 = 5$
$24^3 \times 48$	1.20317(58)(84)	1.2282(9)(16)	1.2537(9)(23)	1.2785(11)(31)	1.3023(11)(25)	1.3254(12)(29)
$32^3 \times 48$	1.20396(47)(69)	1.21821(61)(64)	1.23263(65)(70)	1.24685(69)(79)	1.26077(74)(94)	1.2746(08)(11)
$48^3 \times 64$	1.2032(07)(11)	1.2096(11)(22)	1.2162(11)(21)	1.2227(12)(22)	1.2290(12)(21)	1.2354(13)(21)
$L = \infty$	1.20359(41)(61)					

representative hadronic label (first column in Table II) indicating one component of their hadronic level wave function. To determine which SU(3) irreducible representations (irreps) are present in the correlation functions, the states are acted on by the quadratic and cubic SU(3) Casimir operators, and by V-spin, U-spin, and isospin raising and lowering operators, the results of which are presented in Table II (eigenvalues of the Casimir operator for relevant SU(3) irreps are tabulated in Appendix A). Because of the overall antisymmetric nature of allowed quark-level wave functions, a number of the constructed interpolating operators give rise to correlation functions that contain only one SU(3) irrep, while others contain more than one.

Given the blocks discussed in the previous section and the quark- and hadron-level wave functions introduced previously, the contractions are performed using an algorithm that is described in more detail in Ref. [36]. For a given set of quantum numbers, denoted by $\mathcal{Q}$, we have a basis of $N_{\rm wf}$ hadron-level and quark-level wave functions, $\Psi_i^{(h)}$ and $\Psi_i^{(q)}$, respectively, for $i = 1, \ldots, N_{\rm wf}$. Note that $N_{\rm wf}$ depends on $\mathcal{Q}$. In this work the spatial wave function at the source is restricted to a single point. In addition, the single-baryon interpolating fields are restricted to the upper spin components (in the Dirac basis) only. These two restrictions drastically reduce both the size of the space of allowed quark-level wave functions, and the number of terms each wave function can have. In all cases, an orthonormal basis of wave functions consistent with the above constraints is obtained. The construction, as well as the simplification of the wave functions, is done automatically with symbolic manipulation. Finally, after the construction of the wave functions, independent checks of transformation properties of these wave functions were performed, confirming that these wave functions transform as

expected. As discussed previously, hadron-level wave functions and hadronic blocks with a given total momentum are used at the sink. These basic building blocks allow for the construction of more interpolating fields at the sink with nontrivial spatial hadronic wave functions. In addition, hadron systems with nonvanishing total momentum can be constructed, since the point sources couple to all momenta.

The contraction algorithm is then straightforward and amounts to selecting the appropriate indices in all possible ways from the hadron blocks building the hadronic-level sink wave function, dictated by the quark-level wave function.[3] For all the systems studied here, the total contraction time was an order of magnitude less than the rest of the calculation. In addition, the biggest contraction burden was because of the large number of terms contributing to the wave functions with a nontrivial spatial part at the sink (moving hadrons at the sink). As an example of the speed of our contraction code, a ^{4}He correlation function can be computed in ~ 0.8 s per time slice on a single core of a dual core AMD Opteron 285 processor.

III. THE PION AND BARYON DISPERSION RELATIONS

In the limit of SU(3)-flavor symmetry, all members of the lightest baryon octet have the same mass, and as such, we compute correlation functions associated with only one of the octet baryons. Similarly all octet pseudoscalar mesons are degenerate, and we refer to them as the pion.

---

[3]We note that the algorithm proposed in Ref. [37] is quite similar to the one we have been using in the production of the results presented here.
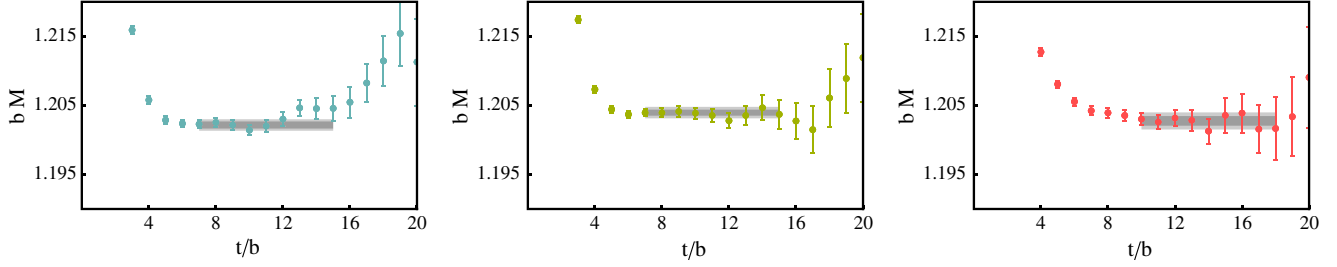
FIG. 1 (color online). The EMPs associated with linear combinations of baryon correlation functions computed with the $24^3 \times 48$ (left), $32^3 \times 48$ (center), and $48^3 \times 64$ (right) ensembles, with momentum $|\mathbf{P}| = 0$. The inner (darker) shaded region corresponds to the statistical uncertainty of the extracted energy, while the outer (lighter) shaded region corresponds to the statistical and fitting systematic uncertainties combined in quadrature. The time extent of each band corresponds to the choice of the fitting interval for each correlation function.
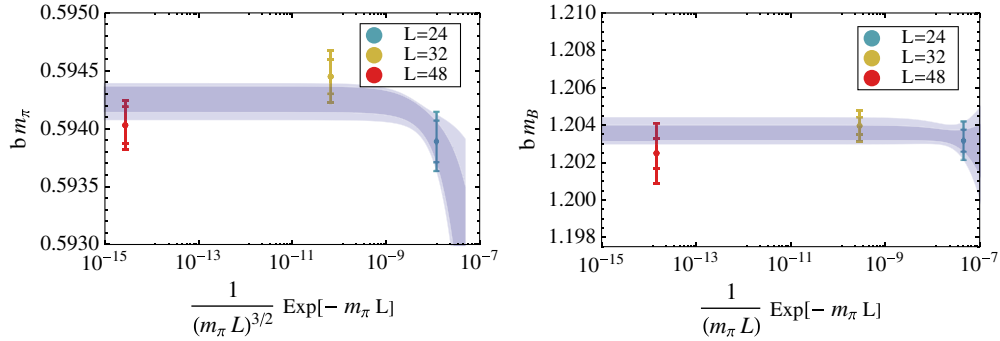
FIG. 2 (color online). The volume dependence of the pion mass (left panel) and the baryon mass (right panel) extracted from the zero-momentum correlation functions. The shaded regions are extrapolations of the form given in Eq. (2).

Linear combinations of single-hadron correlation functions generated from smeared quark sources and either smeared or point sinks are formed for hadrons with a given lattice momentum. The lowest energy eigenvalue can be determined from these correlation functions, the results of which are presented in Table III (pion) and Table IV (baryon), and the baryon effective mass plots (EMPs) are shown in Fig. 1.

For hadrons at rest, the masses of the pion and baryon in finite volume, $m_H^{(V)}(m_\pi L)$, are extrapolated to infinite volume using

$$m_\pi^{(V)}(m_\pi L) = m_\pi^{(\infty)} + c_\pi^{(V)} \frac{e^{-m_\pi L}}{(m_\pi L)^{3/2}} + \cdots,$$

$$M_B^{(V)}(m_\pi L) = M_B^{(\infty)} + c_B^{(V)} \frac{e^{-m_\pi L}}{m_\pi L} + \cdots,$$

(2)

where only the first terms in the finite-volume (FV) expansion are required owing to the large pion mass [38]. The extrapolations to infinite volume are shown as the solid regions in Fig. 2, and the extrapolated values of the pion and octet-baryon mass are presented in Tables III and IV,
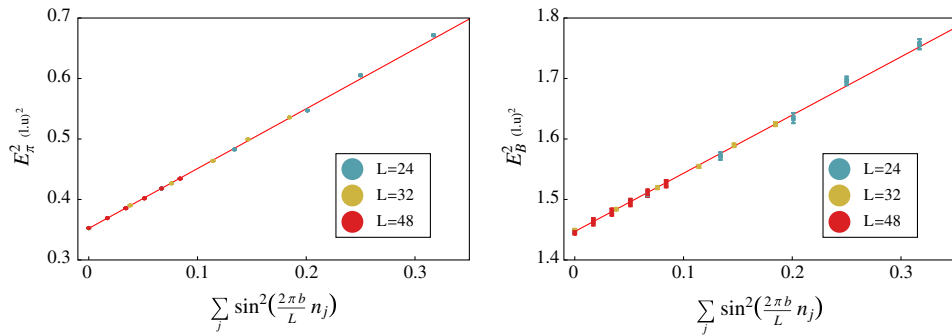

FIG. 3 (color online). The squared energy [in (l.u.)^2] of the single pion and baryon as a function of $\sum_j \sin^2(\frac{2\pi b}{L} n_j)$. The points are the results of the LQCD calculations with the inner (outer) uncertainties being the statistical uncertainties (statistical and systematic uncertainties combined in quadrature). The red curves correspond to the best linear fits.
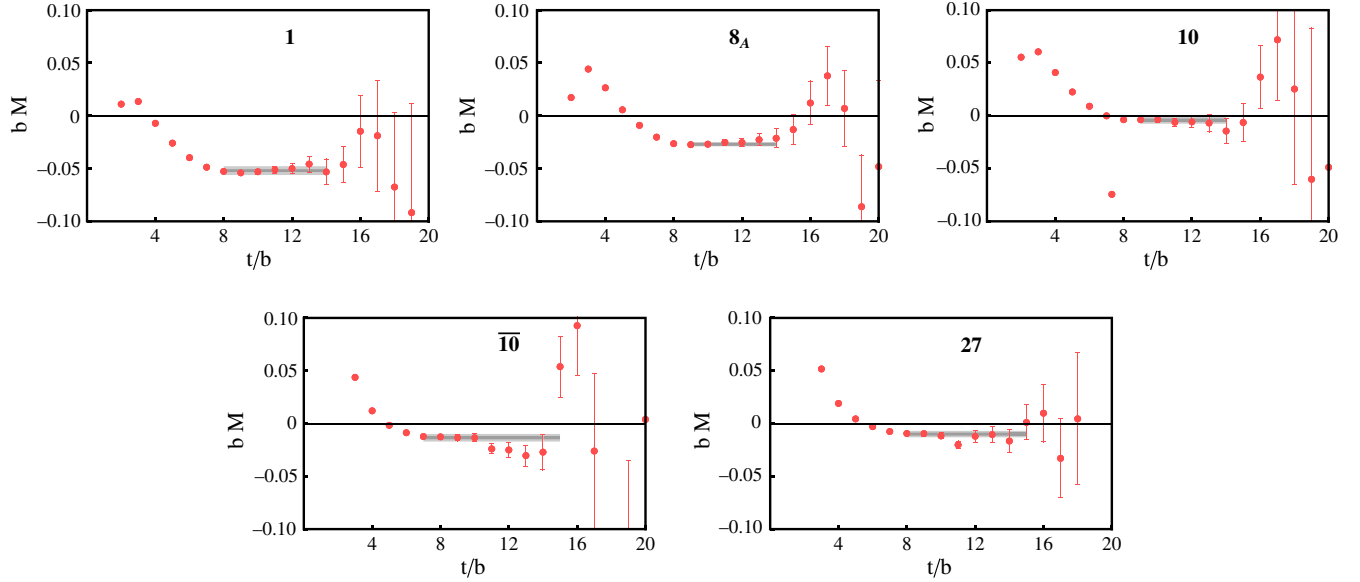
FIG. 4 (color online).   EMPs associated with $|\mathbf{P}| = 0$ two-baryon correlation functions computed with the $48^3 \times 64$ ensemble. The inner (darker) shaded region corresponds to the statistical uncertainty of the extracted energy, while the outer (lighter) shaded region corresponds to the statistical and fitting systematic uncertainties combined in quadrature. The time extent of each band corresponds to the choice of the fitting interval for each correlation function. From left to right, the top row corresponds to the **1**, **8**$_A$, **10** SU(3) irreps (corresponding to the H-dibaryon, $I = 0$ $N\Xi$ in the $^3S_1 - {}^3D_1$ coupled channels and $n\Sigma^-$ in the $^3S_1 - {}^3D_1$ coupled channels, respectively), and the bottom row corresponds to $\overline{\mathbf{10}}$ and **27** (corresponding to the deuteron and dineutron, respectively).

respectively. As expected for calculations with large values of $m_\pi L$, the single-hadron FV effects are very small. The extrapolated pion and octet-baryon masses, using the measured lattice spacing, are $m_\pi = 805.9(0.6)(0.4)(8.9)$ MeV and $m_B = 1.634(0)(0)(18)$ GeV, where the first uncertainty is statistical, the second is the fitting systematic, and the third is attributable to the uncertainty in the lattice spacing.

To have confidence in the extraction of multibaryon binding energies and to be able to quantify one of the systematic uncertainties in these determinations, it is important to determine the single-hadron dispersion relation. The energies of the pion and baryon are shown in Fig. 3 as a function of $\sum_j \sin^2(\frac{2\pi b}{L} n_j)$, where the triplet of integers $\mathbf{n} = (n_1, n_2, n_3)$ is related to the lattice momentum via $|\mathbf{P}|^2 = (\frac{2\pi}{L})^2 |\mathbf{n}|^2$. In these LQCD calculations, the energy of the hadron can be related to its lattice momentum through a dispersion relation of the form

$$(bE_H)^2 = (bM_H)^2 + \frac{1}{\xi_H^2} \sum_j \sin^2\left(\frac{2\pi b}{L} n_j\right), \qquad (3)$$

where the anisotropy parameter, ξ_H (or equivalently the speed of light $c = 1/\xi_H$), is expected to be unity in calculations performed with isotropic lattices.[4] Fitting ξ_H to the energy of the pion and baryon, given in Tables III and IV, respectively, yields $\xi_\pi = 1.0055(57)(26)$ and $\xi_B = 1.019(10)(03)$. Therefore, the dispersion relations provide

---

[4]As the lattice hadronic dispersion relations are *a priori* unknown, they must be calculated. The form given in Eq. (3) is expected to capture the leading momentum dependence.

only a small uncertainty in the extraction of multihadron energies.

IV. TWO-BODY SYSTEMS

In general, the two-body states can be classified by isospin, strangeness, parity, and angular momentum. In the limit of SU(3)-flavor symmetry, the energy eigenstates can also be classified by SU(3) quantum numbers. The lowest-lying baryons transform as **8** under SU(3), and, therefore, the two-body states have degeneracies determined by the dimensionality of the irreps in the product

$$\mathbf{8} \otimes \mathbf{8} = \mathbf{27} \oplus \mathbf{10} \oplus \overline{\mathbf{10}} \oplus \mathbf{8}_S \oplus \mathbf{8}_A \oplus \mathbf{1}. \qquad (4)$$

As the wave functions of such systems are totally antisymmetric, the s-wave $^1S_0$ channels transform under SU(3) as $\mathbf{27} \oplus \mathbf{8}_S \oplus \mathbf{1}$, while the $^3S_1 - {}^3D_1$ coupled channels

TABLE V.   Two-body binding energies (MeV) calculated with the $24^3 \times 48$ ensemble. The first uncertainty is statistical, the second is the fitting systematic, and the third is because of the lattice spacing.

SU(3) irrep	$|\mathbf{n}| = 0$	$|\mathbf{n}| = 1$	$|\mathbf{n}| = 2$
1	77.7(1.8)(3.2)(0.8)	67.2(2.5)(2.5)(0.8)	85.0(3.1)(4.0)(0.9)
8$_A$	40.1(1.7)(2.9)(0.4)	26.5(1.8)(3.6)(0.3)	46.7(2.0)(3.2)(0.5)
10	11.4(1.8)(4.0)(0.1)	6.3(1.9)(4.4)(0.1)	15.3(2.2)(4.5)(0.1)
$\overline{\mathbf{10}}$	25.4(2.6)(4.7)(0.3)	16.0(2.7)(5.9)(0.2)	40.7(3.6)(7.4)(0.5)
27	17.8(1.7)(2.8)(0.2)	6.9(1.8)(3.8)(0.1)	28.5(2.3)(3.8)(0.3)

TABLE VI. Two-body binding energies (MeV) calculated with the $32^3 \times 48$ ensemble. The first uncertainty is statistical, the second is the fitting systematic, and the third is because of the lattice spacing.

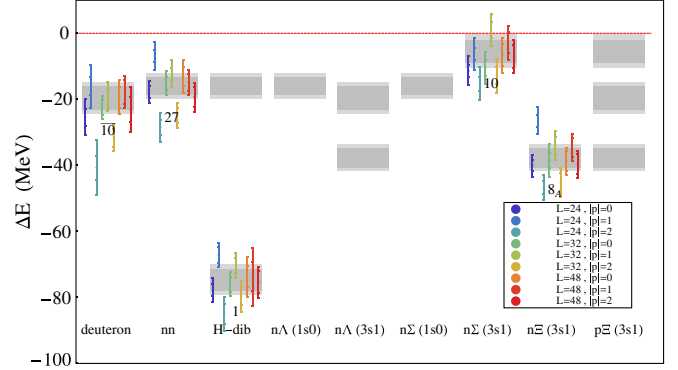| SU(3) irrep	$|\mathbf{n}| = 0$	$|\mathbf{n}| = 1$	$|\mathbf{n}| = 2$
1	76.0(2.3)(2.8)(0.8)	70.3(2.3)(3.1)(0.7)	79.6(2.6)(3.9)(0.9)
8_A	38.5(2.3)(4.4)(0.4)	34.0(2.6)(3.4)(0.4)	45.2(3.0)(3.1)(0.5)
10	10.5(2.5)(4.1)(0.1)	1.1(2.4)(4.2)(0.0)	12.9(2.6)(4.5)(0.1)
$\overline{10}$	22.5(2.3)(2.6)(0.2)	19.2(2.3)(3.7)(0.2)	31.6(2.7)(3.2)(0.3)
27	15.1(2.0)(2.0)(0.2)	12.3(1.9)(3.6)(0.1)	24.9(2.2)(3.1)(0.3)

FIG. 5 (color online). Binding energies in the $A = 2$ systems relative to two noninteracting baryons ($B = -\Delta E$). The points and associated uncertainties are the results of the LQCD calculations given in Tables V, VI, and VII. The dark (statistical uncertainty) and light (statistical and systematic uncertainties combined in quadrature) horizontal bands denote the average of the bindings calculated on the $48^3 \times 64$ ensemble, which are taken as the infinite-volume estimate. Where only bands are shown, SU(3) symmetry has been used to determine the spectrum.

transform as $\mathbf{10} \oplus \overline{\mathbf{10}} \oplus \mathbf{8}_A$. The source structures we have employed, in which the quark-level operators reside at one point in the spatial volume, have vanishing overlap with the $\mathbf{8}_S$ irrep, and as a result, we are unable to determine the energy of this two-body irrep. Correlation functions are not constructed directly in terms of their SU(3) transformation properties, but the contributing SU(3) irreps can be deduced from their structure: $\overline{\mathbf{10}}$ from the deuteron, $\mathbf{27}$ from the dineutron, $\mathbf{1} \oplus \mathbf{27}$ from the H-dibaryon (the $\mathbf{8}_S$ is absent), $\mathbf{10}$ from $n\Sigma^-$ in the $^3S_1 - {}^3D_1$ coupled channels, and $\mathbf{8}_A$ from $I = 0$ $N\Xi$ in the $^3S_1 - {}^3D_1$ coupled channels. EMPs extracted from the two-body correlation functions for systems at rest calculated with the $48^3 \times 64$ ensemble are shown in Fig. 4. The energies of states that are negatively shifted relative to two free baryons are presented in Tables V, VI, and VII, respectively, and displayed in Fig. 5.

The energies of the states that are presented in this work, along with their statistical uncertainties, are determined from a single-parameter correlated χ^2-minimization procedure performed over a specific time interval of EMPs and from exponential fits to the correlation functions directly, with covariance matrices determined with either jackknife or bootstrap. The systematic uncertainty that is assigned to these energies is determined by varying the fit interval over a range of values consistent with the identified plateau region.

A number of scattering states with positive energy shifts relative to two free baryons have also been identified using different correlation functions, but their uncertainties are large enough to preclude clean extraction of scattering

phase shifts using Lüscher's method [39,40], and we defer analysis of these states to a later time when adequate statistics have been accumulated.

In sufficiently large volumes, the binding momentum associated with a two-body bound state at rest in the lattice volume will scale as

$$\kappa(L) = \kappa_0 + \frac{6Z_\psi^2}{L} e^{-\kappa_0 L} + \cdots, \qquad (5)$$

where κ_0 is the infinite-volume binding momentum, $\kappa_0 = \sqrt{M_B B}$, where B is the binding energy and Z_ψ is the residue of the bound-state pole [39–41]. Analogous FV scaling formulas for systems moving in the lattice volume are known [27], but at this order in the expansion they differ from the relation in Eq. (5) only by the coefficient of the second term. In the $32^3 \times 48$ and $48^3 \times 64$ lattice volumes, the energies of the two-body bound states do not exhibit statistically significant volume dependence. Consequently, using Eq. (5) to determine the infinite-volume binding energies does not provide a refinement over simply taking the binding energies determined in the $48^3 \times 64$ ensemble,

TABLE VII. Two-body binding energies (MeV) calculated with the $48^3 \times 64$ ensemble. The first uncertainty is statistical, the second is the fitting systematic, and the third is because of the lattice spacing. The second to last column corresponds to an average of the $|\mathbf{n}| = 0$, 1, 2 calculations, which is taken to be the infinite-volume value. The last column gives the value of κ_0 times the spatial lattice size for $L = 48$.

SU(3) irrep	$|\mathbf{n}| = 0$	$|\mathbf{n}| = 1$	$|\mathbf{n}| = 2$	$L = \infty$	$\kappa_0 L$
1	73.7(3.3)(5.1)(0.8)	73.7(4.4)(7.6)(0.8)	75.4(3.3)(3.3)(0.8)	74.6(3.3)(3.3)(0.8)	12.3
8_A	38.7(2.9)(2.9)(0.4)	34.6(2.8)(3.1)(0.4)	39.7(3.0)(2.7)(0.4)	37.7(3.0)(2.7)(0.4)	8.8
10	6.6(3.4)(4.1)(0.0)	2.8(3.1)(4.1)(0.0)	7.0(3.4)(3.7)(0.0)	5.5(3.4)(3.7)(0.0)	3.3
$\overline{10}$	19.7(3.1)(4.1)(0.2)	17.8(3.6)(3.1)(0.2)	23.1(3.9)(5.5)(0.2)	19.5(3.6)(3.1)(0.2)	6.3
27	13.1(2.8)(4.3)(0.2)	14.9(2.7)(2.7)(0.2)	19.3(2.9)(3.3)(0.2)	15.9(2.7)(2.7)(0.2)	5.7

TABLE VIII. Two-body energy splittings, $E_{I_1} - E_{I_2}$ (MeV), between different multiplets calculated with the $32^3 \times 48$ ensemble. The column refers to representation I_1 and the row to representation I_2. The first uncertainty is statistical, the second is the fitting systematic, and the third is because of the lattice spacing.

$I_2 \backslash I_1$	$\mathbf{8}_A$	$\mathbf{10}$	$\overline{\mathbf{10}}$	$\mathbf{27}$
$\mathbf{1}$	34.3(0.7)(1.2)(0.4)	65.9(0.4)(0.9)(0.7)	49.3(1.4)(1.7)(0.5)	55.4(1.2)(1.8)(0.6)
$\mathbf{8}_A$	-	31.0(0.8)(1.6)(0.3)	14.2(1.1)(2.0)(0.2)	20.5(1.2)(2.3)(0.2)
$\mathbf{10}$	-	-	$-17.7(1.4)(2.2)(0.2)$	$-11.0(1.4)(2.4)(0.1)$
$\overline{\mathbf{10}}$	-	-	-	5.8(1.0)(1.0)(0.1)

and the latter is used as the best estimate of the infinite-volume binding energies, the results of which are shown in Table VII. The expected differences between the infinite-volume bindings and those in the $48^3 \times 64$ ensemble can be estimated from the values of $\kappa_0 L$ given in Table VII. With the exception of the state in the $\mathbf{10}$ irrep, the states are small enough compared to the lattice volume to make the finite-volume effects negligible.

There are a few important results that should be highlighted. The deuteron is found to be substantially more deeply bound in the present calculations, $B_d^{n_f=3} = 19.5(3.6)(3.1)(0.2)$ MeV, than in the quenched calculations [8] in which a binding energy of $B_d^{n_f=0} = 9.1(1.1) \times (0.5)$ MeV at a similar pion mass is found. The H-dibaryon is found to be deeply bound with $B_H = 74.6(3.3)(3.3) \times (0.8)$ MeV, approximately twice as bound as the result found by HALQCD [17] at a similar quark mass. In recent work we reported that the $n\Sigma^-$ interaction in the $^3S_1 - ^3D_1$ channel was extremely repulsive at a pion mass of $m_\pi \sim 390$ MeV [24], consistent with the phase-shift analysis of experimental data at the physical pion mass. At the SU(3) symmetric point, we find that this state has moved close to threshold and is even consistent with being bound, indicating that there is significant light quark mass dependence in this channel at the heavier quark masses (beyond the regime of applicability of the relevant EFT).

As the calculations have been performed at the SU(3) symmetric point, the states discussed above provide a nearly complete set of two-baryon ground states, with only the $\mathbf{8}_S$ irrep being absent. Furthermore, since the determinations of the various energy levels in the two-body sector are correlated, their differences can be determined more precisely than their individual values. In Table VIII we present the splittings between the various irreps. The energy difference between $\overline{\mathbf{10}}$ and $\mathbf{27}$ corresponds to the deuteron-dineutron mass difference. This splitting is found to be small, and consistent with zero within the uncertainties of the calculation. Theoretically, it has been established from SU(2) that these states become degenerate in the large-N_c limit of QCD [42], with a fractional splitting [and violation of Wigner's SU(4) symmetry] that scales as $1/N_c^2$. Extending the argument to the strange sectors shows that the other splittings are only $1/N_c$ suppressed, and not $1/N_c^2$ suppressed [42]. Such scalings are consistent with what we have found, but verification of the scaling will require significantly higher statistics in the calculations.

V. THREE-BODY SYSTEMS

The correlation functions for the three-body systems are generated using the procedure described previously. As is the case for two-body systems, the states in the spectrum for each system can be classified by their SU(3) quantum numbers in the limit of SU(3)-flavor symmetry. The three-body states can be assigned to the SU(3) irreps in $\mathbf{8} \otimes \mathbf{8} \otimes \mathbf{8}$, which can be straightforwardly constructed as

$$\mathbf{8} \otimes \mathbf{8} \otimes \mathbf{8} = \mathbf{64} \oplus 2\,\mathbf{35} \oplus 2\,\overline{\mathbf{35}} \oplus 6\,\mathbf{27} \oplus 4\,\mathbf{10} \oplus 4\,\overline{\mathbf{10}} \oplus 8\,\mathbf{8} \oplus 2\,\mathbf{1}.$$

(6)

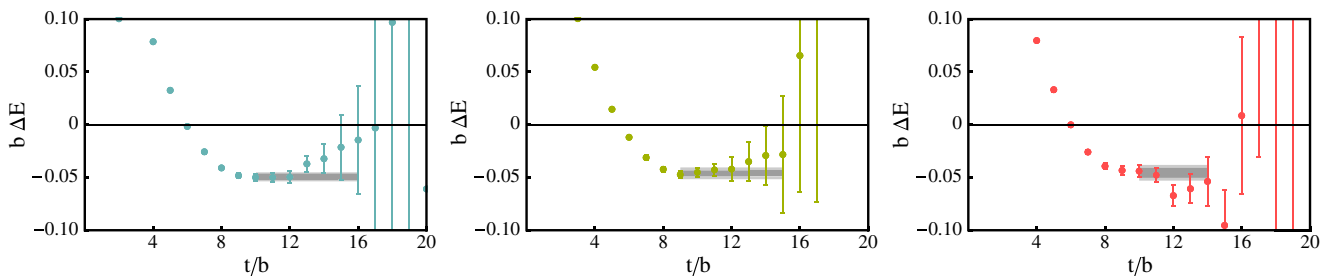FIG. 6 (color online). EMPs associated with $J^\pi = \frac{1}{2}^+$ ^{3}He (^{3}H) $|\mathbf{P}| = 0$ correlation functions computed with the $24^3 \times 48$ (left), $32^3 \times 48$ (center), and $48^3 \times 64$ (right) ensembles. The inner (darker) shaded region corresponds to the statistical uncertainty of the extracted energy, while the outer (lighter) shaded region corresponds to the statistical and fitting systematic uncertainties combined in quadrature.

TABLE IX. The calculated $J^\pi = \frac{1}{2}^+$ binding energy of ^{3}He (^{3}H) in the $24^3 \times 48$ ensemble. The first uncertainty is statistical, the second is the fitting systematic, and the third is because of the lattice spacing.

^{3}He	$|\mathbf{n}|^2 = 0$	$24^3 \times 48$ $|\mathbf{n}|^2 = 1$	$|\mathbf{n}|^2 = 2$
Ground state (MeV)	65.4(5.1)(4.4)(0.7)	42.8(3.8)(8.9)(0.4)	46.3(5.3)(6.7)(0.5)

TABLE X. The calculated $J^\pi = \frac{1}{2}^+$ binding energy of ^{3}He (^{3}H) in the $32^3 \times 48$ ensemble. The first uncertainty is statistical, the second is the fitting systematic, and the third is because of the lattice spacing.

^{3}He	$|\mathbf{n}|^2 = 0$	$32^3 \times 48$ $|\mathbf{n}|^2 = 1$	$|\mathbf{n}|^2 = 2$
Ground state (MeV)	63.2(3.9)(7.0)(0.7)	52.9(5.7)(9.9)(0.6)	55.7(6.4)(10.1)(0.6)

TABLE XI. The calculated $J^\pi = \frac{1}{2}^+$ binding energy of ^{3}He (^{3}H) in the $48^3 \times 64$ ensemble. The first uncertainty is statistical, the second is the fitting systematic, and the third is because of the lattice spacing.

^{3}He	$|\mathbf{n}|^2 = 0$	$48^3 \times 64$ $|\mathbf{n}|^2 = 1$	$|\mathbf{n}|^2 = 2$
Ground state (MeV)	61.9(8.9)(10.9)(0.7)	53.0(7.1)(8.0)(0.6)	50.0(6.1)(9.2)(0.6)

However, the local sources constructed from only the upper components of the quark fields produce correlation functions containing a subset of these irreps,

$$\mathbf{8} \otimes \mathbf{8} \otimes \mathbf{8} \to \mathbf{35} \oplus \overline{\mathbf{35}} \oplus 2\,\mathbf{27} \oplus \mathbf{10} \oplus \overline{\mathbf{10}} \oplus 2\,\mathbf{8} \oplus \mathbf{1}, \quad (7)$$

and further decomposition into states with $J^\pi = \frac{1}{2}^+$ and $J^\pi = \frac{3}{2}^+$ gives

$$(\mathbf{8} \otimes \mathbf{8} \otimes \mathbf{8})_{J^\pi = 1/2^+} \to \mathbf{35} \oplus \overline{\mathbf{35}} \oplus \mathbf{27} \oplus \mathbf{8},$$
$$(\mathbf{8} \otimes \mathbf{8} \otimes \mathbf{8})_{J^\pi = 3/2^+} \to \mathbf{27} \oplus \mathbf{10} \oplus \overline{\mathbf{10}} \oplus \mathbf{8} \oplus \mathbf{1}. \quad (8)$$

It is clear from the SU(3) irreps contributing to the three-body systems that, with our source structure, a given correlation function contains contributions from multiple SU(3) irreps. With a relatively small number of states identified with the present set of correlation functions, the SU(3) classification of states is difficult to establish from the spectra alone. More generally, it is expected that the spectrum of states in any given correlation function becomes increasingly complicated with increasing numbers of baryons even when constrained by SU(3)-flavor symmetry. As the focus of this work is systems containing only a small number of strange quarks, we have chosen to use the same notation as in hypernuclear spectroscopy. States in ^{3}He (same as ^{3}H by isospin symmetry), $^3_\Lambda$He (same as $^3_\Lambda$H and $nn\Lambda$ by isospin symmetry), the isosinglet $^3_\Lambda$H, and the isotriplet $^3_\Sigma$He have been identified in the three-body sector.

Correlation functions calculated with LQCD will contain not only contributions from the ground state and excited states of the bound nuclei but also continuum states that consist of all possible subclusterings of the baryons. For instance, the correlation functions used to extract the ^{3}He nuclear states will also contain contributions from the deuteron-proton and diproton-neutron in addition to
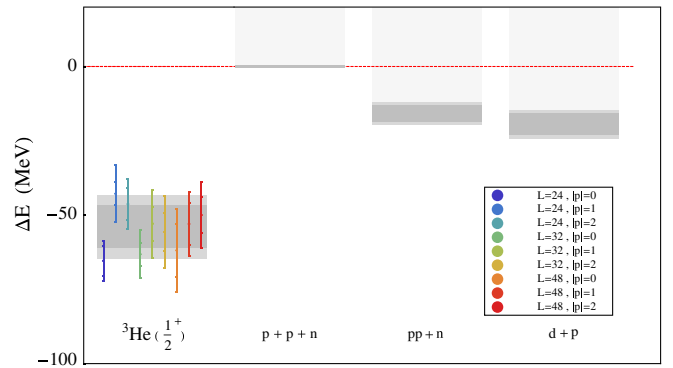

FIG. 7 (color online). The bound-state energy levels in the $J^\pi = \frac{1}{2}^+$ ^{3}He (^{3}H) sector. The points and their associated uncertainties correspond to the energies of the states extracted from the correlation functions with the quantum numbers of the ground state of ^{3}He. The locations of the scattering thresholds associated with noninteracting deuteron-proton, diproton-neutron, and proton-proton-neutron continuum states, determined from the single-hadron spectrum and the two-body binding energies given in Table VII, are shown.
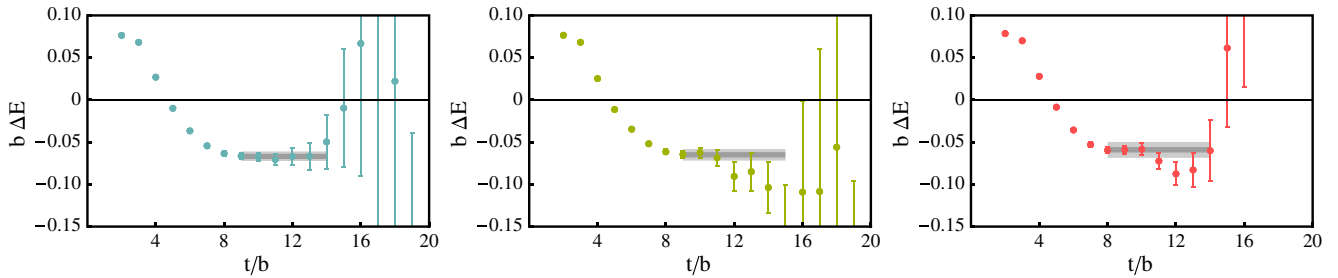
FIG. 8 (color online).   The EMPs associated with a $J^\pi = \frac{3}{2}^+$ hypertriton ($^3_\Lambda$H) correlation function computed with the $24^3 \times 48$ (left), $32^3 \times 48$ (center), and $48^3 \times 64$ (right) ensembles, with momentum $|\mathbf{P}| = 0$. The inner (darker) shaded region corresponds to the statistical uncertainty of the extracted energy, while the outer (lighter) shaded region corresponds to the statistical and fitting systematic uncertainties combined in quadrature.

the proton-proton-neutron continuum states. With sufficient precision in the calculation, one will be able to use these levels to extract, for instance, the deuteron-proton scattering phase shift [26]. Given that the two-body sector is well established, the spectrum of such continuum states can be approximately constructed. Clearly, states of the ^{3}He nucleus can be cleanly identified only when they are not close in energy to the expected location of noninteracting continuum states. The generalization of this discussion applies to other systems composed of three or more baryons. In Appendix B, an example of the expected FV scattering-state spectrum is constructed for each of the volumes used in this analysis, demonstrating the extent of this problem in large volumes.

A. $I = \frac{1}{2}$, $J^\pi = \frac{1}{2}^+$: ^{3}H and ^{3}He

In nature, the $I = \frac{1}{2}$, $J^\pi = \frac{1}{2}^+$ ground state of the ^{3}He nucleus is the only bound state of two protons and a neutron, and it is known to be dominantly composed of two protons in a $^1S_0$ state coupled to an s-wave neutron. Four ^{3}He correlation functions, resulting from different source structures defined by $s = 0$, $I = \frac{1}{2}$, and $J^\pi = \frac{1}{2}^+$ quantum numbers transforming as a $\overline{\mathbf{35}}$ of SU(3), have been constructed.[5] EMPs obtained from correlation functions in each of the three ensembles, from which the energy of the lowest-lying ^{3}He states have been determined, are shown in Fig. 6.

The ^{3}He bound-state energies on the ensembles are given in Tables IX, X, and XI and are shown in Fig. 7 along with the thresholds for noninteracting continuum states.[6] The exact form of infinite-volume extrapolation of three- and higher-body bound-state energies is as yet unknown, though expected to be exponential (see Refs. [43–45] for related discussions). For the current study, we simply average the results obtained from the system at rest and from the boosted systems on the

$48^3 \times 64$ ensemble to provide an estimate of the infinite-volume binding energy of

$$B^{(\infty)}(^3\text{He}) = 53.9(7.1)(8.0)(0.6) \text{ MeV}. \quad (9)$$

The energy of this state is significantly lower than any of the expected continuum states, based upon where they would lie in the spectrum in the absence of interactions. Therefore, we conclude that this is the ground state of ^{3}He.

While it is tempting to compare these results with the experimental spectrum of ^{3}He, one should refrain at present, since these calculations are performed in the SU(3) limit of QCD and without electromagnetism. The ground-state binding energy will receive a shift because of the electromagnetic interaction between the two protons. On the other hand, the exact isospin symmetry directly relates this spectrum to that of the triton. In nature the triton binding energy per nucleon is $B/A \sim 2.83$ MeV, while at the SU(3) symmetric point we find that $B/A \sim 24$ MeV, more than an order of magnitude larger.

The ^{3}He ground-state energy that we have calculated in this $n_f = 3$ calculation is substantially different from that obtained with quenched calculations at a comparable pion mass [9], which find an infinite-volume extrapolated value of $B^{(\infty)}_{n_f=0}(^3\text{He}) = 18.2(3.5)(2.9)$ MeV. A likely explanation for the difference is quenching artifacts, which are unlikely to cancel between the bound system and the threshold states. The difference in the total energy (not the binding energy) of the ^{3}He ground state between the two calculations is of $\mathcal{O}(1\%)$, smaller than the differences observed between single-hadron masses in quenched and unquenched calculations [46]. Additionally, the contributions from continuum states that must be present in both calculations at some level (see Appendix B) may pollute the extraction of the ^{3}He ground state, particularly in large volumes.

B. $I = 0$, $J^\pi = \frac{1}{2}^+$, and $J^\pi = \frac{3}{2}^+$: $^3_\Lambda$H—The Hypertriton

The hypertriton, $^3_\Lambda$H, with the quantum numbers of $np\Lambda$ and $I = 0$ is the simplest hypernucleus produced in the

---

[5]The only possible SU(3) irrep with these quantum numbers is $\overline{\mathbf{35}}$.

[6]Finite-volume effects will lead to small shifts in these thresholds.

TABLE XII. The calculated $J^\pi = \frac{3}{2}^+$ binding energies in $^3_\Lambda$H. "g.s." denotes the ground state. The energies in the $J^\pi = \frac{1}{2}^+$ channel are the same as those of ^{3}He by SU(3) symmetry; see Tables IX, X, and XI. The first uncertainty is statistical, the second is the fitting systematic, and the third is because of the lattice spacing.

$^3_\Lambda$H	$24^3 \times 48$	$32^3 \times 48$	$48^3 \times 64$
$J^\pi = \frac{3}{2}^+$ g.s. (MeV)	90.8(4.5)(6.5)(1.0)	89.6(4.6)(8.9)(1.0)	82(8)(12)(1)

laboratory, having a total binding energy of $B \sim 2.35$ MeV. With a Λ-separation energy of just $B^\Lambda \sim 0.13$ MeV, it is consistent with a Λ weakly bound to a deuteron. The ground state has $J^\pi = \frac{1}{2}^+$ and has been identified as a member of the $\overline{\mathbf{35}}$ of flavor SU(3) [47]. It continues to be the focus of experimental efforts, for instance, in heavy-ion collisions at RHIC [48] and the HypHI project at GSI, where in the latter it is being used as a "phase-zero" calibration nucleus for the production and detection systems [49]. We have calculated correlation functions in both the $J^\pi = \frac{1}{2}^+$ and $J^\pi = \frac{3}{2}^+$ channels and have identified the lowest-lying state in each. Two of the

correlation functions associated with the $J^\pi = \frac{1}{2}^+$ channel are pure $\overline{\mathbf{35}}$ and are in the same irrep as ^{3}He, and hence the energy of the identified states are the same. Further, the $J^\pi = \frac{3}{2}^+$ channel is pure $\overline{\mathbf{10}}$. EMPs in the $J^\pi = \frac{3}{2}^+$ channel from these correlation functions are shown in Fig. 8, from which the energies of the lowest-lying states have been determined, and are given in Table XII. The EMPs in the $J^\pi = \frac{1}{2}^+$ channel are not shown, as they are identical to those of ^{3}He, shown in Fig. 6. The extracted spectra of bound states are shown in Fig. 9. Taking the results obtained in the $48^3 \times 64$ ensemble to be the best estimate of the $^3_\Lambda$H infinite-volume binding energies gives

$$B^{(\infty)}(^3_\Lambda H(1/2^+)) = 53.9(7.1)(8.0)(0.6) \text{ MeV,}$$
$$B^{(\infty)}(^3_\Lambda H(3/2^+)) = 82(8)(12)(1) \text{ MeV,} \tag{10}$$

where we have used the ^{3}He result for the $J^\pi = \frac{1}{2}^+$ binding energy, which includes calculations of boosted systems.

The observed states are significantly below the scattering thresholds and are consistent with a bound $^3_\Lambda$H nucleus at these values of the quark masses in the absence of electromagnetism. Interestingly, the lowest energy state is in the $J^\pi = \frac{3}{2}^+$ spin channel. As the measurements of the two spin states are correlated, the spin splitting can be extracted with high precision, resulting in

$$B^{(\infty)}(^3_\Lambda H(3/2^+)) - B^{(\infty)}(^3_\Lambda H(1/2^+))$$
$$= 26.2(2.3)(5.5)(0.3) \text{ MeV.} \tag{11}$$

C. $I = 1$, $J^\pi = \frac{1}{2}^+$: $^3_\Lambda$He, $^3_\Lambda\tilde{H}$, and $nn\Lambda$

The isotriplet of states,[7] $^3_\Lambda$He, $^3_\Lambda\tilde{H}$, and $nn\Lambda$, are degenerate in the absence of electromagnetism and in the limit of exact isospin symmetry, and can have $J^\pi = \frac{1}{2}^+$ and $J^\pi = \frac{3}{2}^+$. The $J^\pi = \frac{1}{2}^+$ is expected to be the lowest-lying state, with a significant component of the wave function having the two nucleons in the $^1S_0$ channel coupled to Λ. The $J^\pi = \frac{3}{2}^+$ state cannot have such a $NN\Lambda$ configuration in its wave function by the Pauli principle without placing the baryons in orbital excitations but will have configurations of the form of two nucleons in the $^3S_1 - {}^3D_1$ channel coupled to Σ^+. In the SU(3) limit, this can be nearby in
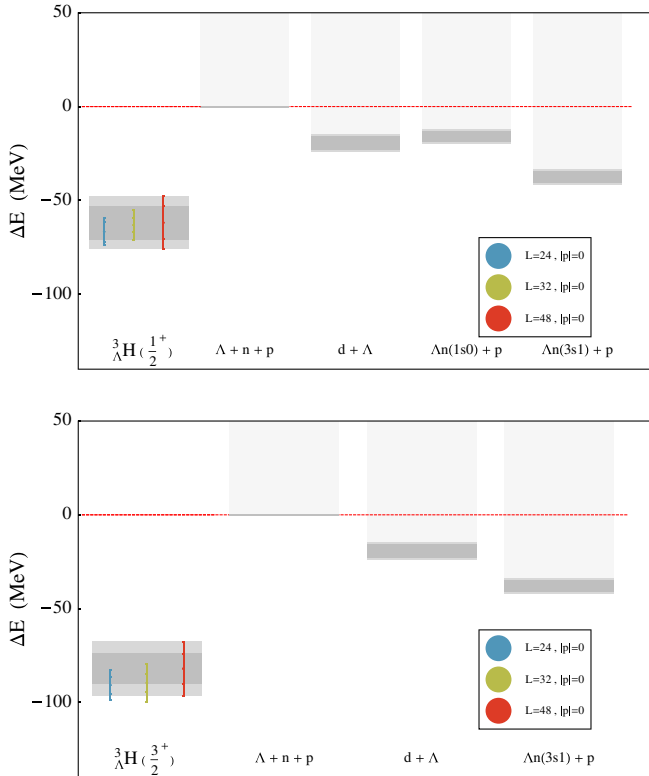

FIG. 9 (color online). The bound-state energy levels in the $J^\pi = \frac{1}{2}^+$ (upper panel) and $J^\pi = \frac{3}{2}^+$ (lower panel) hypertriton ($^3_\Lambda$H) sector. The points and their associated uncertainties correspond to the energies of the states extracted from the correlation functions with the quantum numbers of the ground state of $J^\pi = \frac{1}{2}^+$ and $J^\pi = \frac{3}{2}^+$ $^3_\Lambda$H. The locations of the energy levels associated with noninteracting continuum states, determined from the two-body binding energies given in Table VII, are shown.
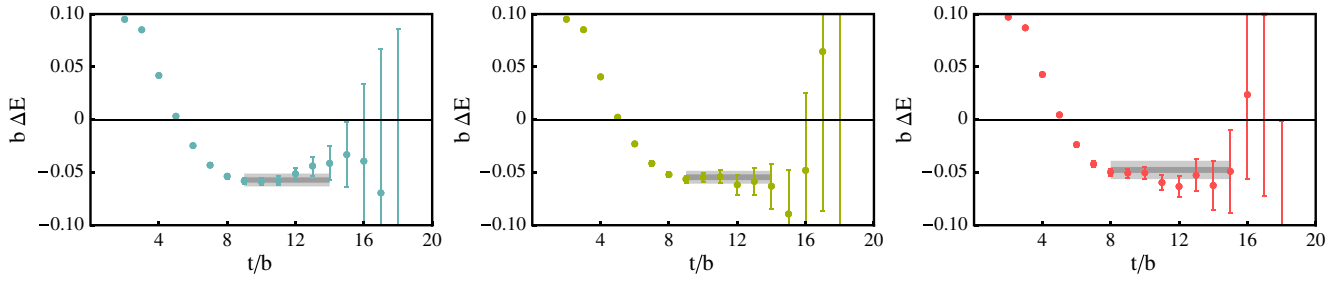
---

[7]We refer to the $np\Lambda$ state with the np coupled to $I = 1$ as $^3_\Lambda\tilde{H}$ to differentiate it from the $^3_\Lambda$H state in which the np couple to $I = 0$.

FIG. 10 (color online). The EMPs associated with one $J^\pi = \frac{1}{2}^+$ $^3_\Lambda$He ($^\Lambda_3$H and $nn\Lambda$) correlation function computed with the $24^3 \times 48$ (left), $32^3 \times 48$ (center), and $48^3 \times 64$ (right) ensembles, with momentum $|\mathbf{P}| = 0$. The inner (darker) shaded region corresponds to the statistical uncertainty of the extracted energy, while the outer (lighter) shaded region corresponds to the statistical and fitting systematic uncertainties combined in quadrature.

energy, but when SU(3) breaking is included, the energy for $J^\pi = \frac{3}{2}^+$ will increase, largely dictated by the $\Sigma - \Lambda$ mass splitting, and become less phenomenologically interesting. Consequently, we will focus first on the $J^\pi = \frac{1}{2}^+$ channel. The EMPs from one of the eight correlation functions of these quantum numbers are shown in Fig. 10, from which the energies of the lowest-lying states have been determined.

The extracted spectrum of bound states is given in Table XIII and shown in Fig. 11. Taking the result obtained on the $48^3 \times 64$ ensemble as the estimate of the infinite-volume binding energy, we find

$$B^{(\infty)}(^3_\Lambda\text{He}(1/2^+)) = 69(5)(12)(0) \text{ MeV.} \quad (12)$$

The ground state is significantly more deeply bound than any of the continuum states, and we identify this as the ground state of the $^3_\Lambda$He nucleus (and hence also bound $^3_\Lambda\tilde{\text{H}}$ and $nn\Lambda$ owing to isospin symmetry). The correlation function from which this ground-state energy was extracted is a superposition of $\overline{\mathbf{35}}$ and $\mathbf{27}$ SU(3) irreps. Another element of the $\mathbf{27}$ irrep is in the $s = -3$ sector, with $I = 1$, $J^\pi = \frac{1}{2}^+$ and with the baryon structure of $N\Xi\Lambda$. One of the correlation functions associated with this state is pure $\mathbf{27}$, and the energy of the lowest-lying state in this correlation function is found to be the same as that in the $^3_\Lambda$He correlation function within the uncertainties of the calculations, suggesting that the $\mathbf{27}$ state is lower in energy than or nearly degenerate with the $\overline{\mathbf{35}}$.

Experimentally, there is no evidence for a bound $^3_\Lambda$He nucleus as the Λ-nucleon interactions are not sufficient to

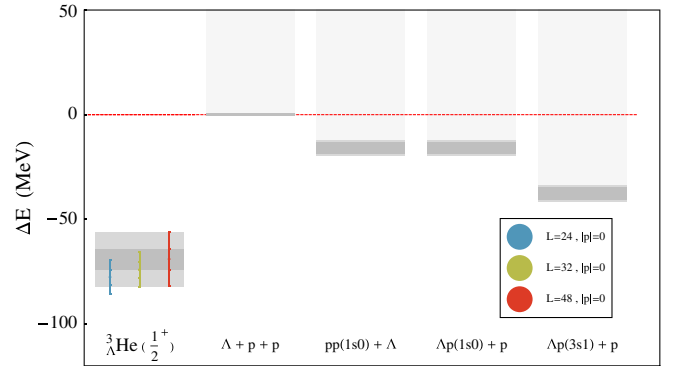
FIG. 11 (color online). The bound-state energy levels in the $J^\pi = \frac{1}{2}^+$ $^3_\Lambda$He ($^\Lambda_3$H and $nn\Lambda$) sector. The points and their associated uncertainties correspond to the energies of the states extracted from the correlation functions with the quantum numbers of the ground state of $^3_\Lambda$He. The locations of the energy levels associated with noninteracting diproton-Λ, ΛN-N, and Λ-N-N continuum states, determined from the two-body binding energies given in Table VII, are shown.

overcome the Coulomb repulsion between the protons. Further, the small binding of the hypertriton, with a significant deuteron-Λ component, strongly suggests that the corresponding $I = 1$ state will be unbound, and it is likely, but yet to be verified, that the $nn\Lambda$ electrically neutral nucleus is also unbound. However, our calculations provide compelling evidence for a bound state in this channel in the limit of SU(3)-flavor symmetry, and we expect that the bound state persists over a range of light-quark masses.

TABLE XIII. The calculated binding energies in $^3_\Lambda$He ($^\Lambda_3$H and $nn\Lambda$). The first uncertainty is statistical, the second is the fitting systematic, and the third is because of the lattice spacing.

$^3_\Lambda$He	$24^3 \times 48$	$32^3 \times 48$	$48^3 \times 64$
Ground state (MeV)	77.6(3.6)(7.5)(0.8)	74.1(3.9)(7.3)(0.8)	69(5)(12)(0)

TABLE XIV. The calculated binding energies in $J^\pi = \frac{3}{2}^+$ $^3_\Sigma$He. The first uncertainty is statistical, the second is the fitting systematic, and the third is because of the lattice spacing.

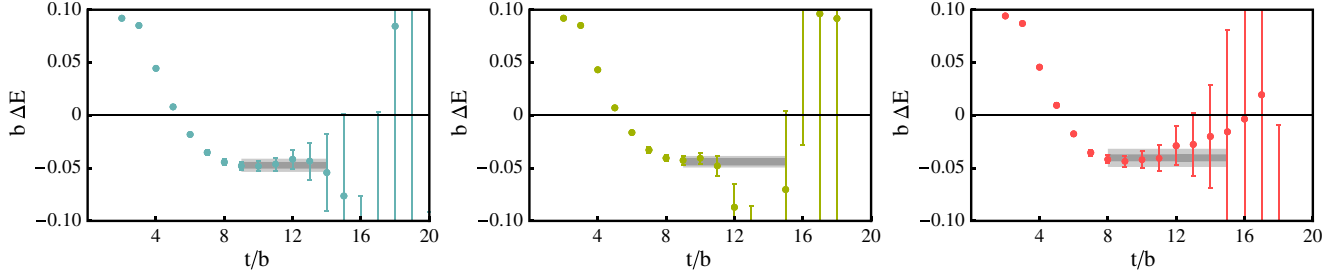| $^3_\Sigma$He	$24^3 \times 48$	$32^3 \times 48$	$48^3 \times 64$
Ground state (MeV)	64.3(4.5)(7.9)(0.7)	58.2(5.2)(7.7)(0.6)	55(6)(10)(1)

FIG. 12 (color online). The EMPs associated with one $J^\pi = \frac{3}{2}^+$ $^3_\Sigma$He correlation function computed with the $24^3 \times 48$ (left), $32^3 \times 48$ (center), and $48^3 \times 64$ (right) ensembles, with momentum $|\mathbf{P}| = 0$. The inner (darker) shaded region corresponds to the statistical uncertainty of the extracted energy, while the outer (lighter) shaded region corresponds to the statistical and fitting systematic uncertainties combined in quadrature.
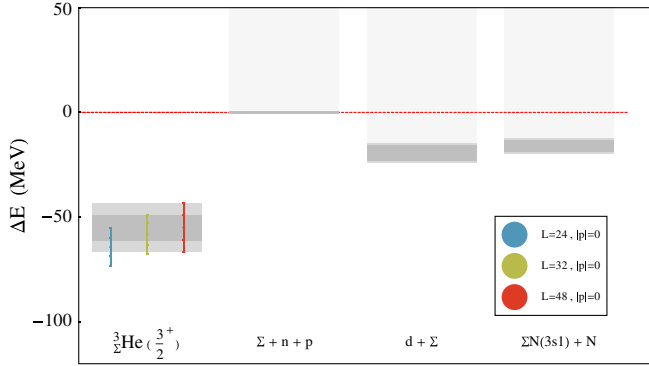
FIG. 13 (color online). The bound-state energy levels in the $J^\pi = \frac{3}{2}^+$ $^3_\Sigma$He sector. The points and their associated uncertainties correspond to the energies of the states extracted from the correlation functions with the quantum numbers of the ground state of $^3_\Sigma$He. The locations of the energy levels associated with noninteracting continuum states, determined from the two-body binding energies given in Table VII, are shown.

D. $I = 1$, $J^\pi = \frac{3}{2}^+$: $^3_\Sigma$He

As discussed above, for the $I = 1$, $s = -1$, $J^\pi = \frac{3}{2}^+$, three-body state, an NNΛ component is forbidden (for all baryons in a relative s wave), and one important contribution to the ground-state wave function is $pn\Sigma$, where the nucleons couple to $I = 0$, $J = 1$, as in $^3_\Lambda$H. As yet, the only observed Σ hypernucleus is $^4_\Sigma$He ($ppn\Sigma^0$) [50,51], but at the SU(3) point it is possible that this three-body system binds. The sources used to generate this correlation function transform as **27** under SU(3)[8] and result in EMPs that exhibit clear plateaus. The ground-state energies extracted from the three ensembles are given in Table XIV, and the associated EMPs are shown in Fig. 12. The ground-state energy and the anticipated continuum thresholds based

upon the noninteracting two-body energies are shown in Fig. 13.

VI. FOUR-BODY SYSTEMS

There are a large number of four-body systems and states that could be explored theoretically with LQCD at the SU(3) symmetric point, dictated by the product of four **8**'s,

$$\mathbf{8} \otimes \mathbf{8} \otimes \mathbf{8} \otimes \mathbf{8} = 8\,\mathbf{1} \oplus 32\,\mathbf{8} \oplus 20\,\mathbf{10} \oplus 20\,\overline{\mathbf{10}} \oplus 33\,\mathbf{27}$$
$$\oplus\, 2\,\mathbf{28} \oplus 2\,\overline{\mathbf{28}} \oplus 15\,\mathbf{35} \oplus 15\,\overline{\mathbf{35}} \oplus 12\,\mathbf{64}$$
$$\oplus\, 3\,\mathbf{81} \oplus 3\,\overline{\mathbf{81}} \oplus \mathbf{125}, \tag{13}$$

giving a total of 166 lowest-lying states (one per distinct irrep) with distinguishable quantum numbers. The local sources that have been used in this work to generate correlation functions project onto a subset of the irreps,

$$(\mathbf{8} \otimes \mathbf{8} \otimes \mathbf{8} \otimes \mathbf{8})_{J^\pi=0^+} \to \mathbf{1} \oplus \mathbf{27} \oplus \overline{\mathbf{28}},$$
$$(\mathbf{8} \otimes \mathbf{8} \otimes \mathbf{8} \otimes \mathbf{8})_{J^\pi=1^+} \to \mathbf{8} \oplus \mathbf{10} \oplus \overline{\mathbf{10}} \oplus \overline{\mathbf{35}}, \tag{14}$$
$$(\mathbf{8} \otimes \mathbf{8} \otimes \mathbf{8} \otimes \mathbf{8})_{J^\pi=2^+} \to \mathbf{8} \oplus \mathbf{27},$$

which greatly reduces the complexity of individual correlation functions. To restrict ourselves to systems that are currently of phenomenological importance, we explore systems containing up to two strange quarks only, the isosinglet ^{4}He, the isodoublet $^4_\Lambda$H and $^4_\Lambda$He, the isosinglet $^4_{\Lambda\Lambda}$H, and the isotriplet $^4_{\Lambda\Lambda}$He, $^4_{\Lambda\Lambda}$H, and $nn\Lambda\Lambda$.

A. $I = 0$, $J^\pi = 0^+$: ^{4}He

In nature, the ^{4}He nucleus is anomalously deeply bound when compared to nuclei nearby in the periodic table, because of its closed shell structure, with a total binding energy of $B \sim 28$ MeV, or a binding energy per nucleon of $B/A \sim 7$ MeV. We anticipate that at the SU(3) symmetric point, the binding energy of ^{4}He will be even deeper given the bindings of the deuteron and dineutron found in the two-body sector. Two of the ^{4}He correlation functions, resulting from different source structures defined by

---

[8]This **27** irrep is different from that in the $J^\pi = \frac{1}{2}^+$ channel. In principle the ground state of the system could reside in the **64** irrep, but this is not accessible with our present operator structure.
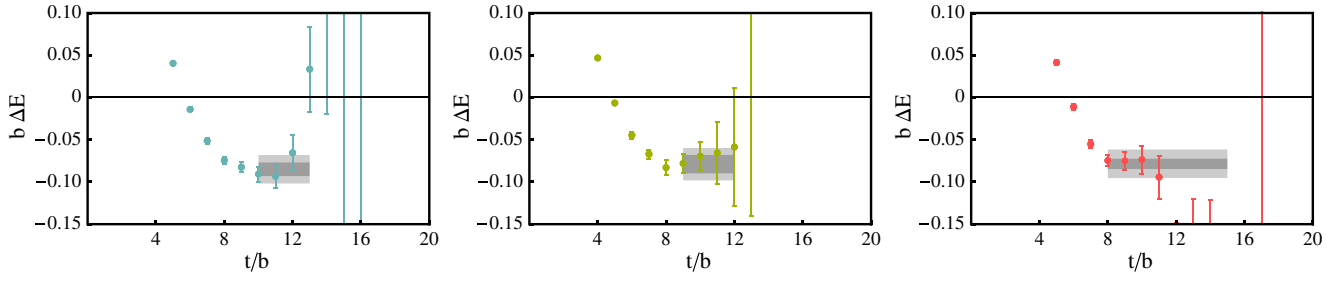
FIG. 14 (color online). EMPs associated with a $|\mathbf{P}| = 0$ $J^\pi = 0^+$ ^{4}He correlation function computed with the $24^3 \times 48$ (left), $32^3 \times 48$ (center), and $48^3 \times 64$ (right) ensembles. The inner (darker) shaded region corresponds to the statistical uncertainty of the extracted energy, while the outer (lighter) shaded region corresponds to the statistical and fitting systematic uncertainties combined in quadrature.

$s = 0$, $I = 0$, and $J^\pi = 0^+$ quantum numbers, transform as an element of the $\overline{\mathbf{28}}$ irrep of SU(3).[9] EMPs of one of these correlation functions are shown in Fig. 14, from which the energies of the lowest-lying states have been determined. The extracted spectrum of bound states, only calculated for the system at rest in the lattice volume, is given in Table XV and shown in Fig. 15. Also shown in Fig. 15 are the thresholds of noninteracting continuum states, based upon the two-body and three-body bound-state spectra. Using the result obtained on the $48^3 \times 64$ ensemble as an estimate of the binding energy in infinite volume, we find

$$B^{(\infty)}(^4\text{He}) = 107(12)(21)(1) \text{ MeV}. \qquad (15)$$

While this state is somewhat more deeply bound than any continuum state, the precision of the calculation is not sufficient to unambiguously distinguish the state from the $n + {}^3$He continuum. To eliminate this ambiguity in state identification, further calculations are required, and additional source structure should be used to increase the size of the basis of correlation functions.

The ^{4}He ground-state energy that we have calculated in this $n_f = 3$ calculation is substantially different from that obtained with quenched calculations at a comparable pion mass [9], which find an infinite-volume extrapolated value of $B^{(\infty)}_{n_f=0}(^4\text{He}) = 27.7(7.8)(5.5)$ MeV, close to the experimental value.

B. $I = \frac{1}{2}$, $J^\pi = 0^+$: $^4_\Lambda$He and $^4_\Lambda$H

In nature, the $^4_\Lambda$He hypernucleus has been well studied experimentally and theoretically. The Λ-separation energy of the $^4_\Lambda$He $J^\pi = 0^+$ ground state is measured to be $S_\Lambda = 2.39(0.03)$ MeV, and for the $J^\pi = 1^+$ first excited state is $S_\Lambda = 1.24(0.05)$ MeV. These two lowest-lying states are consistent with the Λ coupled to a ^{3}He $J^\pi = \frac{1}{2}^+$ core. A recent review of this system can be found in Ref. [52].

We have calculated correlation functions in the $J^\pi = 0^+$ channel, which should provide the ground state, but not the

nearby $J^\pi = 1^+$ first excited state. The sources employed to produce the correlation functions are elements of the same $\overline{\mathbf{28}}$ irrep of SU(3) as those of ^{4}He, and hence the extracted states have the same energy.[10] The EMPs from these correlation functions are the same as those shown in Fig. 14, from which the energies of the lowest-lying states have been determined, and are the same as those in Table XV. The spectrum in this channel, and a subset of associated continuum states, are the same as those in Fig. 15. There are no continuum states from other SU(3) irreps lying lower than those associated with the ^{4}He spectrum (assuming that we have correctly identified the ground states in the three-body sector). However, because of the presence of different SU(3) irreps in this channel, the spectrum of excited states of the nucleus, and the continuum states, is expected to be different from that in the ^{4}He channel.

As is the case for ^{4}He, while the lowest-lying state extracted from the correlation functions has a central value that is lower than any of the noninteracting continuum states, the precision of the calculation is not sufficient to completely exclude the possibility that it is a continuum state, e.g. ^{3}He $+ \Lambda$, or $^3_\Lambda$He $+$ N. The extrapolated binding energy is given in Eq. (15).

C. $I = 1$, $J^\pi = 0^+$: $^4_{\Lambda\Lambda}$He, $^4_{\Lambda\Lambda}$H, and $nn\Lambda\Lambda$

At the SU(3) symmetric point, with a deeply bound H-dibaryon, bound dineutron, and attractive Λn interaction, we naively expect to find that $^4_{\Lambda\Lambda}$He and its isospin partners are bound. This is in contrast to the situation at the physical point, where a doubly strange hypernucleus that is stable against strong decay has not been conclusively observed (for recent reviews of the status of experimental investigations into doubly strange hypernuclei see, for example, Refs. [52–54]). The states in $^4_{\Lambda\Lambda}$He (with $s = -2$ and $I = 1$) and its isospin partners can reside in the **27,**

---

[9]The $\overline{\mathbf{28}}$ is the only allowed $I = 0$, $s = 0$, $A = 4$ irrep.

[10]The $s = -1$, $I = \frac{1}{2}$ systems of various spin configurations have components transforming in the $\overline{\mathbf{81}}$ and **125** irreps that are inaccessible to our operator construction, but that may in principle contain the ground state of this system.

TABLE XV. The calculated binding energies in ^{4}He. The first uncertainty is statistical, the second is the fitting systematic, and the third is because of the lattice spacing.

^{4}He	$24^3 \times 48$	$32^3 \times 48$	$48^3 \times 64$
Ground state (MeV)	115(11)(20)(1)	107(15)(20)(1)	107(12)(21)(1)

$\overline{\mathbf{28}}$, $\overline{\mathbf{35}}$, $\overline{\mathbf{81}}$, **64**, and **125** irreps of SU(3). However, the sources employed in this work produce correlation functions in the $\overline{\mathbf{28}}$ and **27** irreps only, and therefore the complete spectrum cannot be definitively determined. EMPs from one of the correlation functions are shown in Fig. 16, from which the energies of the lowest-lying states have been determined. The extracted ground-state energies, only calculated for the system at rest in the lattice volume, are given in Table XVI and shown in Fig. 17. The energy of the lowest state in the correlation function with contributions from $\overline{\mathbf{28}}$ and **27** is found to be the same within

uncertainties with that from a pure **27** correlation function. The energy of the lowest state in $\overline{\mathbf{28}}$ is that of the ground state of ^{4}He by SU(3) symmetry and is significantly larger than that of **27**, and clearly **27** is dominating the large-time behavior of the mixed correlation function. Using the result obtained on the $48^3 \times 64$ ensemble as an estimate of the binding energy in infinite volume, we find that

$$B^{(\infty)}(_{\Lambda\Lambda}^4\mathrm{He}) = 156(16)(21)(2) \text{ MeV.} \qquad (16)$$

The ground state is more bound than any continuum state (although we have been unable to cleanly isolate the ground state of the doubly strange three-body hypernuclei), and we identify this as the ground state of the $_{\Lambda\Lambda}^4$He, $_{\Lambda\Lambda}^4$H, $nn\Lambda\Lambda$ isotriplet. However, it is possible that this is an excited state of the nucleus, with irreps other than $\overline{\mathbf{28}}$ and **27** containing a lower-energy state. Further, it is also possible that this state is a continuum scattering state associated with N + $_{\Lambda\Lambda}^3$H. Clearly, further calculations are also required to unambiguously distinguish the energy of the **27** ground state from that of the $\overline{\mathbf{28}}$ excited state.

VII. FIVE-BODY SYSTEMS

There are a plethora of five-body systems that can be explored theoretically at the SU(3) symmetric point, dictated, in part, by the product of five **8**'s,

$$\begin{aligned}
\mathbf{8} \otimes \mathbf{8} \otimes \mathbf{8} \otimes \mathbf{8} \otimes \mathbf{8} = {}& 32\,\mathbf{1} \oplus 145\,\mathbf{8} \oplus 100\,\mathbf{10} \oplus 100\,\overline{\mathbf{10}} \\
& \oplus 180\,\mathbf{27} \oplus 20\,\mathbf{28} \oplus 20\,\overline{\mathbf{28}} \oplus 100\,\mathbf{35} \\
& \oplus 100\,\overline{\mathbf{35}} \oplus 94\,\mathbf{64} \oplus 5\,\mathbf{80} \oplus 5\,\overline{\mathbf{80}} \\
& \oplus 36\,\mathbf{81} \oplus 36\,\overline{\mathbf{81}} \oplus 20\,\mathbf{125} \\
& \oplus 4\,\mathbf{154} \oplus 4\,\overline{\mathbf{154}} \oplus \mathbf{216}.
\end{aligned} \qquad (17)$$

In this work, we explore one five-body state that can be produced by local quark-level operators, involving only their upper components, with all five baryons in a relative s wave. Unfortunately, this system, with $s = -3$, has not been experimentally observed.

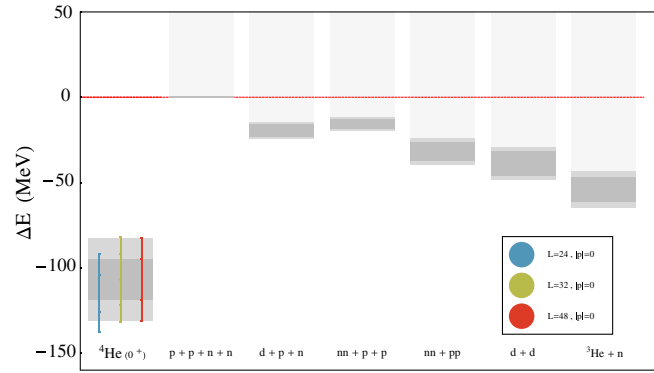FIG. 15 (color online). The bound-state energy levels in the $J^\pi = 0^+$ ^{4}He sector. The points and their associated uncertainties correspond to the energies of the states extracted from the correlation functions with the quantum numbers of the ground state of ^{4}He. The locations of the energy levels associated with noninteracting N-^{3}He, d-d, dineutron-dineutron, dineutron-N-N, d-N-N, and N-N-N-N continuum states, determined from the two-body binding energies given in Table VII and the three-body energies given in Eq. (9), are shown.
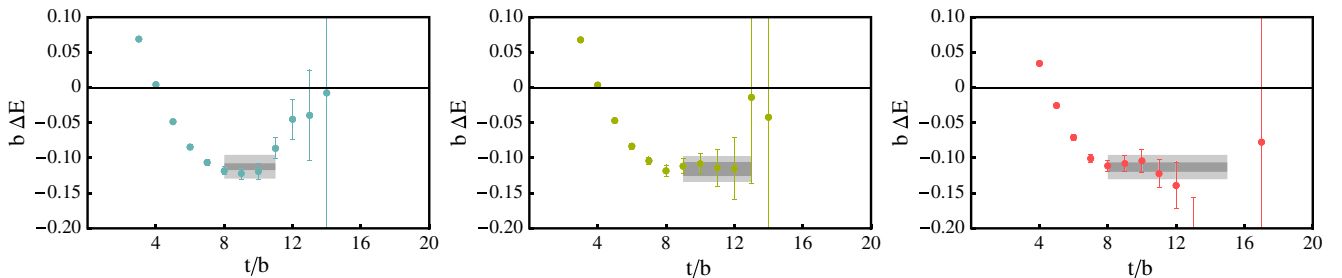

FIG. 16 (color online). The EMPs associated with one of the eight $J^\pi = 0^+$ $_{\Lambda\Lambda}^4$He correlation functions computed with the $24^3 \times 48$ (left), $32^3 \times 48$ (center), and $48^3 \times 64$ (right) ensembles, with momentum $|\mathbf{P}| = 0$. The inner (darker) shaded region corresponds to the statistical uncertainty of the extracted energy, while the outer (lighter) shaded region corresponds to the statistical and fitting systematic uncertainties combined in quadrature.

TABLE XVI. The calculated binding energies in $_{\Lambda\Lambda}^{4}$He. The first uncertainty is statistical, the second is the fitting systematic, and the third is because of the lattice spacing.

$_{\Lambda\Lambda}^{4}$He	$24^3 \times 48$	$32^3 \times 48$	$48^3 \times 64$
Ground state (MeV)	157(7)(22)(2)	154(14)(19)(2)	156(16)(21)(2)

A. $I = 0$, $J^\pi = \frac{3}{2}^+$: $\Lambda \Xi^0 pnn$

The $\Lambda \Xi^0 pnn$ state has $I = 0$, $s = -3$, $J^\pi = 3/2^+$, and belongs to a $\overline{\mathbf{10}}$ irrep of SU(3). Extending the standard hypernuclear nomenclature, it may be referred to as $_{\Lambda\Xi}^{5}$H. Experimentally, it is not clear how such a state could be produced and, given the two-body interactions, it is not expected to be bound at the physical values of the light-quark masses. The EMPs for this system in each of the
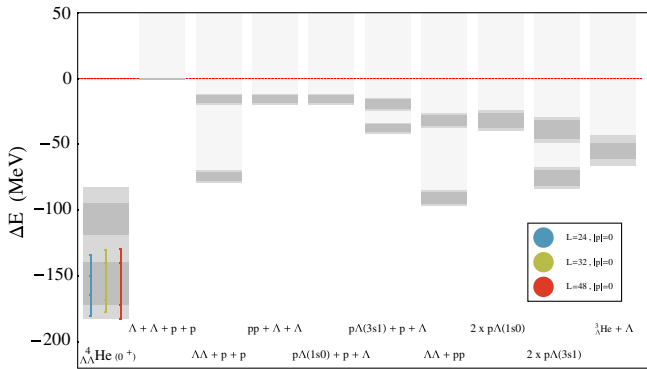
FIG. 17 (color online). The bound-state energy levels in the $J^\pi = 0^+$ $_{\Lambda\Lambda}^{4}$He ($_{\Lambda\Lambda}^{4}$H and $nn\Lambda\Lambda$) sector. The points and their associated uncertainties correspond to the energies of the states extracted from the correlation functions with the quantum numbers of the ground state of $_{\Lambda\Lambda}^{4}$He. The excited state of the $_{\Lambda\Lambda}^{4}$He, in $\overline{\mathbf{28}}$, has the same energy as the ground state of ^{4}He. The locations of the energy levels associated with non-interacting Λ-$_{\Lambda}^{3}$He, $N\Lambda$-$N\Lambda$, H-dibaryon-dineutron, $N\Lambda$-$N\Lambda$, dineutron-Λ-Λ, H-dibaryon-N-N, and Λ-Λ-N-N continuum states, determined from the two-body binding energies given in Table VII and the three-body energies given in Eqs. (9) and (12), are shown.
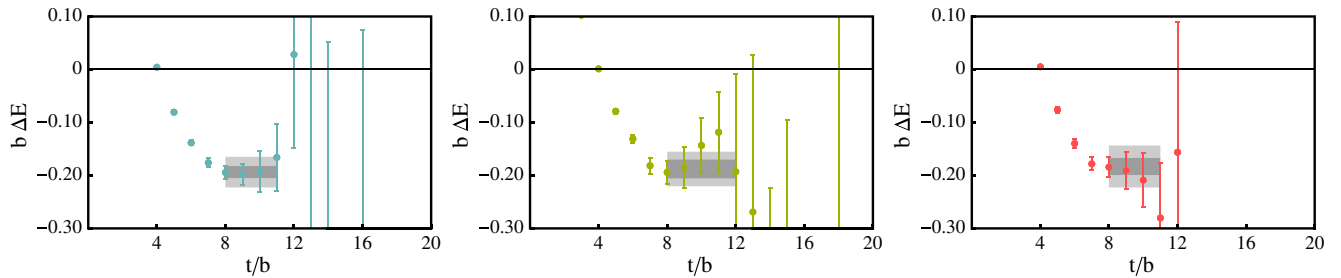
lattice volumes are shown in Fig. 18, from which it is clear that the lowest state is negatively shifted with the energies given in Table XVII. It is not clear that $\overline{\mathbf{10}}$ contains the ground state of the system, or if it corresponds to a continuum state.

While it is interesting to study this state for algorithmic reasons, the states of more importance are those that can be accessed experimentally, those with $s = 0, -1, -2$. These more interesting systems have baryons in a relative p wave, i.e. p-shell nuclei and hypernuclei, and require retaining the lower components of the quark fields in the local operators by parity considerations. Unfortunately, we find that such operators have poor overlap onto such systems, and produce noisy correlation functions. These nuclei can be accessed with nonlocal operators and are the subject of future work.

VIII. SUMMARY AND CONCLUSIONS

We have presented the results of lattice QCD calculations of various of the lightest nuclei and hypernuclei with $A \le 5$ and with light-quark masses at the (unphysical) SU(3)-flavor symmetric point equal to the physical strange-quark mass. These calculations were performed in three lattice volumes with spatial extent 3.4 fm, 4.5 fm, and 6.7 fm, and with one lattice spacing of $b \sim 0.145$ fm. Using a new algorithm to perform the Wick contractions, ground-state energies of a number of nuclear states were determined from one or more correlation function(s) generated from local quark-level operators for systems at rest or moving in the lattice volumes. A summary of the binding energies determined in this work can be found in Table XVIII and is shown in Fig. 19. The approximate binding energy per baryon, which is seen to be significantly larger than found in nature, is also shown in Table XVIII.

In contrast to QCD with the light-quark masses at their physical values, at the SU(3) symmetric point all two-body channels except possibly $N\Sigma(^3S_1)$ contain a bound state in their spectrum. The SU(3) $\mathbf{1}$ H-dibaryon is the most deeply bound two-body state, and its excitation, transforming as $\mathbf{27}$ of SU(3), is also bound. The nature of the sources used in this work, each derived from the same light-quark

FIG. 18 (color online). The EMPs of the single correlation function for the $\Lambda \Xi^0 pnn$ state. The inner (darker) shaded region corresponds to the statistical uncertainty of the extracted energy, while the outer (lighter) shaded region corresponds to the statistical and fitting systematic uncertainties combined in quadrature.

TABLE XVII. The calculated binding energies in $_{\Lambda\Xi^0}^{5}$H. The first uncertainty is statistical, the second is the fitting systematic, and the third is because of the lattice spacing.

$_{\Lambda\Xi^0}^{5}$H	$24^3 \times 48$	$32^3 \times 48$	$48^3 \times 64$
Ground state (MeV)	273(19)(39)(3)	255(25)(37)(3)	245(28)(81)

propagator, are such that states in the symmetric $\mathbf{8}_S$ of SU(3) are not produced in the correlation functions, and as such, we are unable to locate these states in the two-body spectrum. The energy splitting between the deuteron and the dineutron is found to be smaller than the splittings to the other SU(3) irreps, consistent with what is found in nature, and the result of a large-N_c analysis. It is interesting to note that the deuteron remains a finely tuned system even at this heavy pion mass. In nature, the ratio of the deuteron binding momentum to the pion mass (which defines the range of the nuclear force) is $\sqrt{M_N B_d}/m_\pi \sim 0.33$, where M_N is the nucleon mass and B_d is the deuteron binding energy. This quantity is exploited as an expansion parameter in the low-energy effective field theory description of nuclear interactions [55]. Our calculations reveal that $\sqrt{M_N B_d}/m_\pi \sim 0.24$ at $m_\pi \sim 800$ MeV, which, by this measure, is even more finely tuned than at the physical light-quark masses.

In the three-body sector, we are able to cleanly identify the $J^\pi = \frac{1}{2}^+$ ground state of ^{3}He and its isospin partner ^{3}H, and the total binding energy is determined to be 53.9(7.1)(8.0)(0.6) MeV. In the case of the hypertriton, $_\Lambda^3$H, the states in both the $J^\pi = \frac{1}{2}^+$ and $J^\pi = \frac{3}{2}^+$ channels are consistent with being bound nuclear states and not continuum states. They are both found to be deeply bound, with the $J^\pi = \frac{3}{2}^+$ state being somewhat more bound than the $J^\pi = \frac{1}{2}^+$ state. This is in contrast to the situation in nature, where the

$J^\pi = \frac{1}{2}^+$ hypertriton is found to be very weakly bound. The $J^\pi = \frac{1}{2}^+$ ground state of $_\Lambda^3$He, and its isospin partners $_\Lambda^3$H and $nn\Lambda$, are cleanly identified, with a binding energy of 69(5)(12)(0) MeV, which is substantially lower than the corresponding continuum states. Further, the $J^\pi = \frac{3}{2}^+$ $_\Sigma^3$He ground state is observed to be more bound than continuum states but is somewhat less phenomenologically interesting, as it does not contain an $NN\Lambda$ component.

In the case of ^{4}He, a bound $J^\pi = 0^+$ ground state has been identified, which, while lower in energy than any of the continuum states, cannot be unambiguously identified as a bound ^{4}He nucleus because of the precision of the calculations. As the sources employed for $_\Lambda^4$He and ^{4}He are in the same SU(3) irrep, their spectra are identical in the present calculations, and as such, this ambiguity is present for $_\Lambda^4$He also. The ground state of $_{\Lambda\Lambda}^4$He and its isospin partners $_{\Lambda\Lambda}^4$H and $nn\Lambda\Lambda$ can be clearly identified, with a binding energy of 156(16)(21)(2) MeV.

Finally, we have calculated correlation functions in an exotic five-baryon channel, with $s = -3$. Significantly more calculations will need to be performed to cleanly identify a ground state in this system, but this calculation has demonstrated that the contractions for five-body systems can now be performed.

It is now clear, but hardly a surprise, that the spectrum of nuclei and hypernuclei change dramatically from light-quark masses at the SU(3) symmetric point to the physical point. While we had already learned this from the recent work on the H-dibaryon, and nucleon-nucleon scattering lengths, this has now been demonstrated to be true for even larger systems. While the binding energy per nucleon of the deuteron (and dineutron) is about 10 MeV, for ^{3}He and ^{4}He it is near 25 MeV. These values are significantly larger than the 1.1 MeV, 2.6 MeV, and 7.0 MeV, respectively, at

TABLE XVIII. Summary of the extracted ground-state binding energies of the nuclei and hypernuclei studied in this work.

| State	A	s	I	J^π	SU(3) irrep	Binding energy [MeV]	$\sim B/A$ [MeV]
d (deuteron)	2	0	0	1^+	$\overline{\mathbf{10}}$	19.5(3.6)(3.1)(0.2)	10
nn (dineutron)	2	0	1	0^+	$\mathbf{27}$	15.9(2.7)(2.7)(0.2)	8
$n\Sigma$	2	-1	$\frac{3}{2}$	1^+	$\mathbf{10}$	5.5(3.4)(3.7)(0.0)	3
H (H-dibaryon)	2	-2	0	0^+	$\mathbf{1}$	74.6(3.3)(3.3)(0.8)	37
$n\Xi$	2	-2	0	1^+	$\mathbf{8}_A$	37.7(3.0)(2.7)(0.4)	19
^{3}He, ^{3}H	3	0	$\frac{1}{2}$	$\frac{1}{2}^+$	$\overline{\mathbf{35}}$	53.9(7.1)(8.0)(0.6)	18
$_\Lambda^3$H (hypertriton)	3	-1	0	$\frac{1}{2}^+$	$\overline{\mathbf{35}}$	53.9(7.1)(8.0)(0.6)	18
$_\Lambda^3$H (hypertriton)	3	-1	0	$\frac{3}{2}^+$	$\overline{\mathbf{10}}$	82(8)(12)(1)	27
$_\Lambda^3$He, $_\Lambda^3\tilde{\text{H}}$, $nn\Lambda$	3	-1	1	$\frac{1}{2}^+$	$\mathbf{27}$	69(5)(12)(0)	23
$_\Sigma^3$He	3	-1	1	$\frac{3}{2}^+$	$\mathbf{27}$	55(6)(10)(1)	18
^{4}He	4	0	0	0^+	$\overline{\mathbf{28}}$	107(12)(21)(1)	27
$_\Lambda^4$He, $_\Lambda^4$H	4	0	0	0^+	$\overline{\mathbf{28}}$	107(12)(21)(1)	27
$_{\Lambda\Lambda}^4$He, $_{\Lambda\Lambda}^4$H, $nn\Lambda\Lambda$	4	0	0	0^+	$\mathbf{27}$	156(16)(21)(2)	39
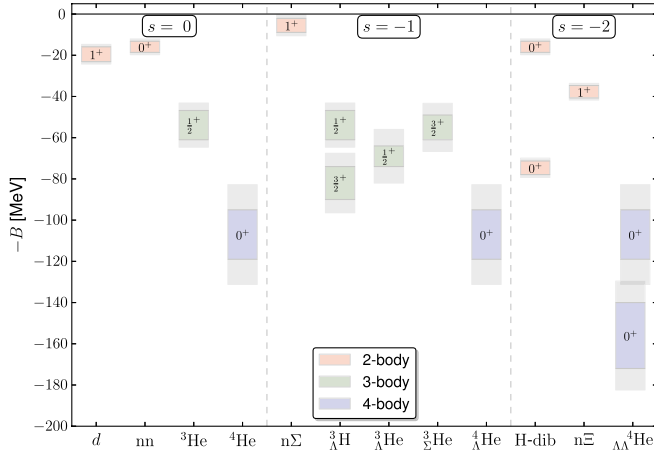
FIG. 19 (color online). A compilation of the nuclear energy levels, with spin and parity J^π, determined in this work.

the physical pion mass. It will be interesting to learn how the various thresholds for binding evolve with the light-quark masses. Providing accurate binding energies for any given light-quark masses will require the inclusion of electromagnetic effects, the leading contributions of which can be determined at the classical level and simply added to the results of the LQCD calculations. A deeper understanding of the origin of the binding energies calculated in this work will require a series of nuclear few-body calculations, which are beyond the scope of the present work. In particular, it is important to understand the relative contribution from the two-body, three-body, and higher-body contributions to the $A \geq 3$ nuclei and hypernuclei, which can only be accomplished using modern few-body techniques.

Our results suggest that quenching in LQCD calculations produces significantly larger errors in the binding of nuclei than it does in the hadron masses. While the differences could be attributable to finite lattice spacing effects and the different quark discretizations, their size is not too surprising given the modifications to the long-range component of the nucleon-nucleon interaction attributable to quenching. It was shown in Ref. [56] that the hairpin interactions that arise in quenched and partially quenched theories generate exponential contributions to the nucleon-nucleon interaction in addition to the usual Yukawa interactions at long distances. Therefore, one anticipates significant modifications to the binding of nuclei, especially for finely tuned systems.

By diversifying and refining the source structure used to generate the correlation functions, the continuum states in each channel can be explored. In the case of two-body continuum states, such as $n + {}^3$He in the ^{4}He channel, the established scattering formalism of Lüscher will allow for the scattering phase shifts in $n + {}^3$He to be rigorously determined from QCD below the inelastic threshold. For the three-body and higher-body continuum states, further

formal developments are required to rigorously determine multibody S-matrix elements.

Lattice QCD has evolved to the point where first-principles calculations of light nuclei are now possible, as demonstrated by the calculations at unphysically heavy light-quark masses presented in this work. The experimental program in hypernuclear physics, and the difficulties encountered in accurately determining rates for low-energy nuclear reactions, warrant continued effort in, and development of, the application of LQCD to nuclear physics. Clearly, calculations at smaller lattice spacings at the SU(3) symmetric point are required to remove the systematic uncertainties in the nuclear binding energies at these quark masses. While not providing quantities that can be directly compared with experiment, these calculations provide valuable information about the quark-mass dependence of spectrum of the lightest nuclei, and hence the nuclear forces, and will shed light on the fine-tunings that are present in nuclear physics. To impact directly the experimental program in nuclear and hypernuclear physics, analogous calculations must be performed at lighter quark masses, ideally at their physical values.

ACKNOWLEDGMENTS

APPENDIX A: CASIMIRS OF SU(3)

To classify the states of the nuclei into irreps of flavor-SU(3), the quark-level sources that generate the nuclear

TABLE XIX. The values of the quadratic and cubic Casimir operators in SU(3), $c_2(m, n)$, and $c_3(m, n)$.

irrep	m	n	c_2	c_3
1	0	0	0	0
3	1	0	$\frac{4}{3}$	$\frac{10}{9}$
3̄	0	1	$\frac{4}{3}$	$-\frac{10}{9}$
6	2	0	$\frac{10}{3}$	$\frac{35}{9}$
6̄	0	2	$\frac{10}{3}$	$-\frac{35}{9}$
8	1	1	3	0
10	3	0	6	9
10̄	0	3	6	-9
27	2	2	8	0
28	6	0	18	45
28̄	0	6	18	-45
35	4	1	12	18
35̄	1	4	12	-18
64	3	3	15	0
81	5	2	20	30
81̄	2	5	20	-30
125	4	4	24	0

correlation functions are acted on with the quadratic and cubic Casimir operators of SU(3),

$$\hat{C}_2 = \sum_a \hat{T}^a \hat{T}^a, \qquad \hat{C}_3 = \sum_{abc} d_{abc}\, \hat{T}^a \hat{T}^b \hat{T}^c. \quad \text{(A1)}$$

The Casimir operators acting on an irrep of SU(3) that has a tensor representation with m upper and n lower indices, $\hat{\theta}^{a_1 \cdots a_m}_{b_1 \cdots b_n}$ of dimensionality

$$d(m, n) = \frac{1}{2}(m + 1)(n + 1)(m + n + 2), \quad \text{(A2)}$$

have eigenvalues

$$c_2(m, n) = \frac{1}{3}(m^2 + n^2 + mn) + m + n,$$

$$c_3(m, n) = \frac{1}{18}(2m + n + 3)(2n + m + 3)(m - n),$$

$$\text{(A3)}$$

the values of which are given in Table XIX for the relevant irreps.

APPENDIX B: THE EXPECTED CONTINUUM STATES IN THE FINITE LATTICE VOLUMES

Given the single-hadron and two-body energies that have been extracted in Secs. III and IV, the continuum states that are expected to arise in the three-body sectors with given quantum numbers can be estimated. Similarly, the information obtained for the three-body systems extracted in Sec. V allows for an estimate of the continuum states in the four-body sector, and so forth in higher-body systems. In the figures in the main text, this information has been presented as the infinite-volume
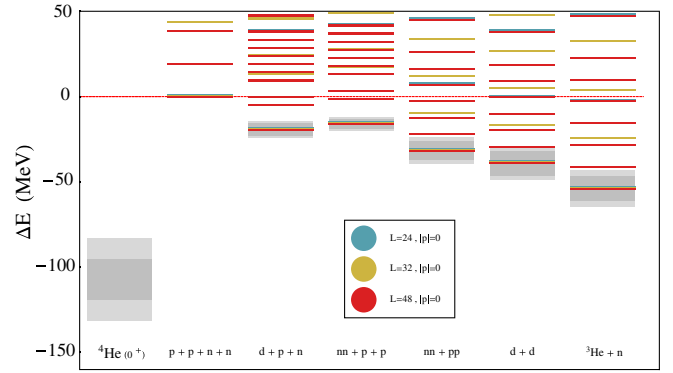

FIG. 20 (color online). Expected energy levels in the $J^\pi = 0^+$ ^{4}He sector. The dark (blue), medium (green), and light (red) lines in each column denote the location of noninteracting continuum levels in the $24^3 \times 48$, $32^3 \times 48$, and $48^3 \times 64$ ensembles, respectively. The location of the states in the $24^3 \times 48$ and $32^3 \times 48$ ensembles have been displaced slightly for demonstrative purposes.

thresholds for the various possible continuum channels. Here, we present an example of the expected spectrum of states in the ^{4}He system in the different lattice volumes used in this work.

For a noninteracting two-component system, composed of nuclei A_1 and A_2, the individual components have only back-to-back momenta,

$$E^{\text{(cont)}}_{A_1, A_2} = \sqrt{M^2_{A_1} + |\mathbf{p}|^2} + \sqrt{M^2_{A_2} + |\mathbf{p}|^2}. \quad \text{(B1)}$$

For three or more cluster continuum states (for example $d + p + n$ in the ^{4}He channel), labeling the clusters A_1, $A_2, \ldots, A_n$, the system has energies permitted by momentum conservation

$$E^{\text{(cont)}}_{A_1, A_2, \ldots, A_n} = \delta^{(3)}\left(\sum_{i=1}^n \mathbf{p}_i\right) \sum_{i=1}^n \sqrt{M^2_{A_i} + |\mathbf{p}_i|^2}, \quad \text{(B2)}$$

with the obvious generalization to systems with a nonzero center-of-mass momentum. These considerations ignore the interactions between the clusters, which will modify the position of the corresponding energy levels. For two-body clusters, it is expected that there will be $\mathcal{O}(1/L^3)$ shifts in the continuum energies, but for higher-body clusters the form of the energy shifts is not known. In Fig. 20 we present the expected (ignoring interactions) FV energy levels in the ^{4}He sector for each of the volumes used in this work.

With more accurate LQCD calculations and additional interpolating operators, we aim to investigate these states in the future. However, this makes clear the difficulty in extracting excited states in nuclei from this type of calculation. The continuum states rapidly accumulate as the lattice volume becomes large, and isolating nuclear excited states above the lowest-lying continuum states will be challenging with current technology and algorithms.

[1] M. Fukugita, Y. Kuramashi, H. Mino, M. Okawa, and A. Ukawa, Phys. Rev. Lett. **73**, 2176 (1994).

[2] M. Fukugita, Y. Kuramashi, M. Okawa, H. Mino, and A. Ukawa, Phys. Rev. D **52**, 3003 (1995).

[3] S. R. Beane, P. F. Bedaque, K. Orginos, and M. J. Savage, Phys. Rev. Lett. **97**, 012001 (2006).

[4] S. R. Beane W. Detmold, H.-W. Lin, T. C. Luu, K. Orginos, M. J. Savage, A. Torok, and A. Walker-Loud (NPLQCD Collaboration), Phys. Rev. D **81**, 054505 (2010).

[5] N. Ishii, S. Aoki, and T. Hatsuda, Phys. Rev. Lett. **99**, 022001 (2007).

[6] S. Aoki, T. Hatsuda, and N. Ishii, Comput. Sci. Discovery **1**, 015009 (2008).

[7] S. Aoki, T. Hatsuda, and N. Ishii, Prog. Theor. Phys. **123**, 89 (2010).

[8] T. Yamazaki, Y. Kuramashi, and A. Ukawa, Phys. Rev. D **84**, 054506 (2011).

[9] T. Yamazaki, Y. Kuramashi, and A. Ukawa, Phys. Rev. D **81**, 111504 (2010).

[10] T. Doi S. Aoki, T. Hatsuda, Y. Ikeda, T. Inoue, N. Ishii, K. Murano, H. Nemura, K. Sasaki, and HAL QCD Collaboration (HAL QCD Collaboration), Prog. Theor. Phys. **127**, 723 (2012).

[11] S. R. Beane, W. Detmold, T. Luu, K. Orginos, A. Parreño, M. Savage, A. Torok, and A. Walker-Loud, Phys. Rev. D **80**, 074501 (2009).

[12] P. de Forcrand and M. Fromm, Phys. Rev. Lett. **104**, 112005 (2010).

[13] S. R. Beane *et al.* (NPLQCD Collaboration), Phys. Rev. Lett. **106**, 162001 (2011).

[14] S. R. Beane, E. Chang, W. Detmold, H. Lin, T. Luu, K. Orginos, A. Parreño, M. Savage, A. Torok, and A. Walker-Loud (NPLQCD Collaboration), Phys. Rev. D **85**, 054511 (2012).

[15] T. Inoue, N. Ishii, S. Aoki, T. Doi, T. Hatsuda, Y. Ikeda, K. Murano, H. Nemura, and K. Sasaki (HAL QCD Collaboration), Phys. Rev. Lett. **106**, 162002 (2011).

[16] T. Inoue (HAL QCD Collaboration), AIP Conf. Proc. **1441**, 335 (2012).

[17] T. Inoue, S. Aoki, T. Doi, T. Hatsuda, Y. Ikeda, N. Ishii, K. Murano, H. Nemura, and K. Sasaki (HAL QCD Collaboration), Nucl. Phys. **A881**, 28 (2012).

[18] S. R. Beane *et al.*, Mod. Phys. Lett. A **26**, 2587 (2011).

[19] P. E. Shanahan, A. W. Thomas, and R. D. Young, Phys. Rev. Lett. **107**, 092004 (2011).

[20] J. Haidenbauer and U.-G. Meissner, Phys. Lett. B **706**, 100 (2011).

[21] V. G. J. Stoks and T. A. Rijken, Phys. Rev. C **59**, 3009 (1999).

[22] G. A. Miller, arXiv:nucl-th/0607006.

[23] J. Haidenbauer and U.-G. Meißner, Phys. Lett. B **684**, 275 (2010).

[24] S. R. Beane, E. Chang, S. D. Cohen, W. Detmold, H.-W. Lin, T. C. Luu, K. Orginos, A. Parreno, M. J. Savage, and A. Walker-Loud, Phys. Rev. Lett. **109**, 172001 (2012).

[25] J. Pochodzalla, Acta Phys. Pol. B **42**, 833 (2011).

[26] S. Bour, S. Koenig, D. Lee, H.-W. Hammer, and U.-G. Meissner, Phys. Rev. D **84**, 091503 (2011).

[27] Z. Davoudi and M. J. Savage, Phys. Rev. D **84**, 114502 (2011).

[28] B. Sheikholeslami and R. Wohlert, Nucl. Phys. **B259**, 572 (1985).

[29] W. Detmold, R. Edwards, B. Joo, T. Luu, S. Meinel, K. Orginos, D. Richards, and A. Walker-Loud (to be published).

[30] C. Morningstar and M. J. Peardon, Phys. Rev. D **69**, 054501 (2004).

[31] R. Hoffmann, A. Hasenfratz, and S. Schaefer, Proc. Sci., LAT2007 (2007) 104.

[32] R. G. Edwards, B. Joo, and H.-W. Lin, Phys. Rev. D **78**, 054501 (2008).

[33] S. Meinel (private communication).

[34] S. Basak, R. Edwards, G. Fleming, U. Heller, C. Morningstar, D. Richards, I. Sato, and S. Wallace [Lattice Hadron Physics (LHPC) Collaboration], Phys. Rev. D **72**, 074501 (2005).

[35] M. I. Buchoff, T. C. Luu, and J. Wasem, Phys. Rev. D **85**, 094511 (2012).

[36] W. Detmold and K. Orginos, arXiv:1207.1452.

[37] T. Doi and M. G. Endres, arXiv:1205.0585 [Comput. Phys. Commun. (to be published)].

[38] S. R. Beane, E. Chang, W. Detmold, H. W. Lin, T. C. Luu, K. Orginos, A. Parreno, M. J. Savage, A. Torok, and A. Walker-Loud, Phys. Rev. D **84**, 014507 (2011).

[39] M. Lüscher, Commun. Math. Phys. **105**, 153 (1986).

[40] M. Lüscher, Nucl. Phys. **B354**, 531 (1991).

[41] S. R. Beane, P. F. Bedaque, A. Parreno, and M. J. Savage, Phys. Lett. B **585**, 106 (2004).

[42] D. B. Kaplan and M. J. Savage, Phys. Lett. B **365**, 244 (1996).

[43] S. Kreuzer and H.-W. Hammer, Phys. Lett. B **694**, 424 (2011).

[44] K. Polejaeva and A. Rusetsky, Eur. Phys. J. A **48**, 67 (2012).

[45] S. Kreuzer and H. W. Grießhammer, Eur. Phys. J. A **48**, 93 (2012).

[46] A. Ali Khan *et al.* (CP-PACS Collaboration), Phys. Rev. D **65**, 054505 (2002); ()**67**, 059901(E) (2003).

[47] B. Ram, Phys. Rev. **141**, 1581 (1966).

[48] J. H. Chen (STAR Collaboration), Nucl. Phys. **A830**, 761c (2009).

[49] T. R. Saito *et al.*, Nucl. Phys. **A881**, 218 (2012).

[50] R. S. Hayano, Phys. Lett. B **231**, 355 (1989).

[51] T. Nagae *et al.*, Phys. Rev. Lett. **80**, 1605 (1998).

[52] A. Gal, Prog. Theor. Phys. Suppl. **186**, 270 (2010).

[53] T. Nagae, Prog. Theor. Phys. Suppl. **185**, 299 (2010).

[54] J. Pochodzalla, A. Botvina, and A. Sanchez Lorente, Proc. Sci., BORMIO2010 (2010) 033.

[55] J.-W. Chen, G. Rupak, and M. J. Savage, Nucl. Phys. **A653**, 386 (1999).

[56] S. R. Beane and M. J. Savage, Phys. Lett. B **535**, 177 (2002).

[57] R. G. Edwards and B. Joo, Nucl. Phys. B, Proc. Suppl. **140**, 832 (2005).